

Journal Pre-proof

Ompalisib Inspired Macrocycles as Dual PI3K/mTOR Inhibitors

Rosa M. Alvarez, Ana Belén García, Concepción Riesco-Fagundo, José I. Martín, Carmen Varela, Antonio Rodríguez Hergueta, Esther González Cantalapiedra, Julen Oyarzabal, Bruno Di Geronimo, Milagros Lorenzo, M Isabel Albarrán, Antonio Cebriá, David Cebrián, Sonia Martínez-González, Carmen Blanco-Aparicio, Joaquín Pastor



PII: S0223-5234(20)31081-3

DOI: <https://doi.org/10.1016/j.ejmech.2020.113109>

Reference: EJMECH 113109

To appear in: *European Journal of Medicinal Chemistry*

Received Date: 11 September 2020

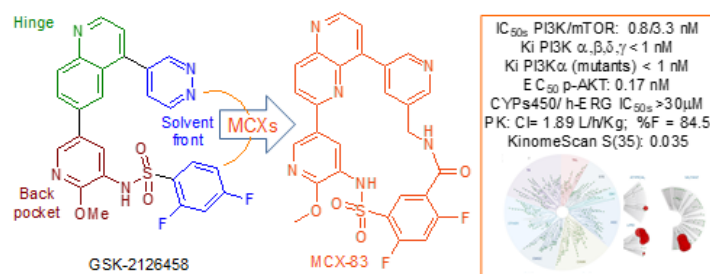
Revised Date: 25 November 2020

Accepted Date: 13 December 2020

Please cite this article as: R.M Alvarez, A.B. García, C. Riesco-Fagundo, J.I. Martín, C. Varela, A.R. Hergueta, E.G. Cantalapiedra, J. Oyarzabal, B. Di Geronimo, M. Lorenzo, M.I. Albarrán, A. Cebriá, D. Cebrián, S. Martínez-González, C. Blanco-Aparicio, J. Pastor, Ompalisib Inspired Macrocycles as Dual PI3K/mTOR Inhibitors, *European Journal of Medicinal Chemistry*, <https://doi.org/10.1016/j.ejmech.2020.113109>.

This is a PDF file of an article that has undergone enhancements after acceptance, such as the addition of a cover page and metadata, and formatting for readability, but it is not yet the definitive version of record. This version will undergo additional copyediting, typesetting and review before it is published in its final form, but we are providing this version to give early visibility of the article. Please note that, during the production process, errors may be discovered which could affect the content, and all legal disclaimers that apply to the journal pertain.

© 2020 Elsevier Masson SAS. All rights reserved.



Journal Pre-proof

Omipalisib Inspired Macrocycles as Dual PI3K/mTOR Inhibitors

*Rosa M^a Alvarez^a, Ana Belén García^a, Concepción Riesco-Fagundo^a, José I. Martín^{a,1},
Carmen Varela^a, Antonio Rodríguez Hergueta^{a,2}, Esther González Cantalapiedra^a, Julen
Oyarzabal^{a,3}, Bruno Di Geronimo^a, Milagros Lorenzo^a, M^a Isabel Albarrán^a, Antonio
Cebriá^a, David Cebrián^{a,4}, Sonia Martínez-González^a, Carmen Blanco-Aparicio^a,
Joaquín Pastor^{a,*}*

^aExperimental Therapeutics Programme, Spanish National Cancer Research Centre (CNIO), C/ Melchor Fernández Almagro 3, E-28029 Madrid, Spain

Corresponding Author

* Joaquín Pastor. Phone: +34 917328000, fax: +34 917328051. E-mail address: jpastor@cnio.es.

Present addresses

¹ Medicinal Chemistry. Diseases of the developing world, GSK. C/ Severo Ochoa, 2, E-28760 Science to Business Technology Park, Spain.

² Centro de Investigación Lilly S.A., Avda. de la Industria, 30, Alcobendas, E-28108, Madrid, Spain.

³ Small Molecule Discovery Platform. Molecular Therapeutics Program, Center for Applied Medical Research, CIMA, University of Navarra, Avda. Pío XII, 55; 31008 Pamplona, Spain.

⁴ Pharmacology unit. Diseases of the developing world, GSK. C/ Severo Ochoa, 2, E-28760 Science to Business Technology Park, Spain.

Abbreviations

ADME-T, absorption, distribution, metabolism, excretion and toxicity; ADP, adenosine diphosphate; APCI, atmospheric pressure chemical ionization; CNS, central nervous system; DCE, dichloroethane; DCM, dichloromethane; DIPEA, *N,N*-diisopropylethylamine; DMAP, 4-dimethylaminopyridine; DME, dimethoxyethane; DMF, *N,N*-dimethylformamide; DMSO, dimethyl sulfoxide; EC₅₀, half maximal effective concentration; ESI, electrospray ionization; EtOAc, ethyl acetate; FDA, food and drug administration; HATU, hexafluorophosphate azabenzotriazole tetramethyl uronium; cHex, cyclohexane; HOAt, 1-hydroxy-7-azabenzotriazole; HPLC, high performance liquid chromatography; HTRF homogeneous time resolved fluorescence; I.V., intravenous; LCMS, liquid chromatography mass spectrometry; MCX(s) (macrocycle(s)); MeOH, methanol; NMP, *N*-methylpyrrolidone; NMR, nuclear magnetic resonance; PDB, protein data bank; PKB, protein kinase B; P.O., per oral; oral administration; PyBOP, (benzotriazol-1-yl-oxytripyrrolidinophosphonium hexafluorophosphate); SAR, structure activity relationship; TEA, triethylamine; TFA, trifluoroacetic acid.

Abstract

Activation of the phosphatidylinositol 3-kinase (PI3K)/mammalian target of rapamycin (mTOR) signaling pathway occurs frequently in a wide range of human cancers and is a main driver of cell growth, proliferation, survival, and chemoresistance of cancer cells. Compounds targeting this pathway are under active development as anticancer therapeutics and some of them have reached advanced clinical trials or been approved by the FDA. Dual PI3K/mTOR inhibitors combine multiple therapeutic efficacies in a single molecule by inhibiting the pathway both upstream and downstream of AKT.

Herein, we report our efforts on the exploration of novel small molecule macrocycles (MCXs) as dual PI3K/mTOR inhibitors. Macrocyclization is an attractive approach used in drug discovery, as the semi-rigid character of these structures could provide improved potency, selectivity and favorable pharmacokinetic properties. Importantly, this strategy allows access to new chemical space thus obtaining a better intellectual property position.

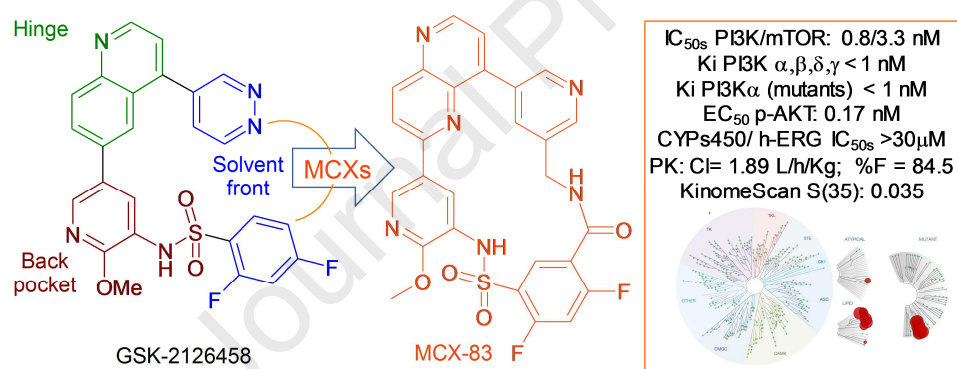
A series of MCXs based on GSK-2126458, a known clinical PI3K/mTOR inhibitor is described. These molecules showed potent biochemical and cellular dual PI3K/mTOR inhibition, demonstrated strong antitumoral effects in human cancer cell lines, and displayed good drug-like properties.

Among them, MCX **83** presented remarkable selectivity against a panel of 468 kinases, high *in vitro* metabolic stability, and favorable pharmacokinetic parameters without significant CYP450 and h-ERG binding inhibition. This profile qualified this compound as a suitable candidate for future *in vivo* PK-PD and efficacy studies in mouse cancer models.

Keywords: Dual PI3K/mTOR inhibitors; anticancer therapies; macrocycles; drug-like properties; selectivity; *in vivo* PK studies.

Highlights:

- Design and synthesis of a new series of MCXs as dual PI3K/mTOR inhibitors.
- Macrocyclization strategy used to tune dual PI3K/mTOR inhibition.
- MCXs with potent biochemical, cellular activity and kinase selectivity.
- MCXs with good drug-like properties.
- MCX **83**, highly potent, selective and orally bioavailable PI3K/mTOR inhibitor.

Graphical Abstract

1. Introduction

The PI3K/AKT/mTOR signaling pathway is implicated in several cellular functions including cell growth, proliferation, differentiation, motility, survival, angiogenesis and intracellular trafficking. Activation of this pathway contributes to the development of tumors such as breast, colorectal and lung cancers and hematologic malignancies and it is involved in resistance to anticancer therapies. PI3Ks is a group of lipid kinases, consisting of two subunits: p85 or p55 regulatory subunits, and p110 catalytic subunit. The PI3K family is divided into classes I, II, and III. Class I PI3Ks in turn are divided into class IA and IB. Class IA PI3K, a heterodimer of p85/p110 subunits, is the type most related to human cancer. Class IA PI3K are divided into p110 α , p110 β and p110 δ isoforms, while p110 γ belongs to class IB PI3K. PIK3CA, the gene encoding the p110 α subunit, is frequently mutated or amplified in many human cancers, being the most common mutations E545K, H1047R and E542K. PI3Ks are activated by receptor tyrosine kinases and Ras and Rho family GTPases. Then, they phosphorylate the 3-hydroxyl position of PIP2 (phosphatidylinositol 4,5-diphosphate) to generate PIP3 (phosphatidylinositol 3,4,5-triphosphate), a secondary messenger that participates in the activation of several downstream effectors, including AKT (PKB) kinase. Subsequently, activated AKT triggers a signal transduction cascade that ultimately stimulates mTOR activity [1].

mTOR is a class IV PI3K protein kinase and is part of two distinct complexes (mTORC1 and mTORC2 both sharing the catalytic activity of mTOR) and plays an integral key role in regulating PI3K/AKT activation and signaling through positive and negative feedback loops [2-4].

Targeting the PI3K/AKT/mTOR pathway is an important therapeutic approach to treat cancer. In this regard, small molecule inhibitors of PI3K include dual PI3K/mTOR

inhibitors, pan-isoforms PI3K inhibitors, and isoform-selective PI3K inhibitors. Several of these molecules have reached advanced clinical trials and the FDA has approved two of them (www.fda.org) [5]. This is the case for the PI3K- δ specific inhibitor Idelalisib (GS-1101, CAL-101) and the selective PI3K- α/δ inhibitor Copanlisib (BAY-80-6946).

Dual inhibitors of PI3K and mTOR target the active catalytic sites of both holoenzymes, inhibiting the pathway both upstream and downstream of AKT. The rationale for PI3K/mTOR dual inhibition as a therapy was based on the observation that persistent mTOR signaling was reported to confer resistance to PI3K inhibition, while selective targeting of the mTOR complex 1 (TORC1) initiates positive feedback leading to PI3K hyperactivation. Dual PI3K/mTOR inhibitors with strong activity toward all p110 isoforms and mTOR combine multiple therapeutic efficacies in a single molecule. Pan-isoform PI3K inhibitors are expected to reduce the risk of drug resistance that might occur in case of treatment with compounds targeting a single p110 isoform and, together with mTOR inhibition, could prevent feedback loop activation of AKT following mTOR inhibition [6, 7].

Macrocyclic versions of small molecules have been used in drug discovery, providing some benefits over the corresponding “open compounds”. There are several examples where the fixation of the bioactive conformation of certain inhibitors by macrocyclization has led to the improvement of their on-target potency. Moreover, macrocyclization can modulate the selectivity against off-targets or, less common, to add a desired target activity. This approach can also modulate ADME-T properties and brain penetration for CNS targeted therapies as it is the case of Crizotinib based MCXs. Last but not least, the design of novel MCXs has been used in the field of drug discovery to access new chemical space, thereby gaining intellectual property [8-12].

It is interesting to highlight that among the plethora of PI3K/mTOR inhibitors reported to date, none of them is a small molecule MCX. In this context, we want to report our efforts on the discovery and exploration of macrocyclic dual PI3K/mTOR inhibitors.

2. Results and discussion

2.1. Design and Synthesis of Inhibitors

As a chemical starting point for the discovery and design of our MCXs we selected the known clinical PI3K/mTOR inhibitor GSK-2126458 (Omipalisib) (Fig.1) [13].

The SAR of this class of inhibitors, and the available crystallographic information have demonstrated the importance of the acceptor N of the central scaffold, which established a key interaction with Val882 in the hinge area of PI3K- γ (Val851 in PI3K- α). Additionally, the “pyridosulfonamide” moiety filled the so-called affinity pocket and produced interactions with Lys833 *via* the sulfonamide group and with Asp841/Tyr867 through a water bridge with its pyridyl N. On the other hand, the C-4 substituent at the quinoline scaffold, which points to the solvent front of PI3K, was less important and even expendable to achieve good activity in this class of inhibitors (Fig. 1A). The structure of GSK-2126458 bound to the kinase domain of mTOR has not been published, however the docking of the inhibitor revealed a similar binding mode as in PI3K (Fig. 1B). The quinoline moiety established contacts with the hinge region of mTOR showing a key interaction with Val2240 and pi-stacking interactions with the exclusive mTOR residue Trp2239. The “pyridosulfonamide” moiety filled the back pocket area, and established interactions with residues such as Lys2187 and Gln2167.

The pyridazine and di-fluoro substituted phenyl fragments of GSK-2126458 are located in the solvent front in both kinases (Fig. 1), and could be used as linkages to design MCXs

capable of retaining the main interactions described above and, therefore, PI3K/mTOR activity.

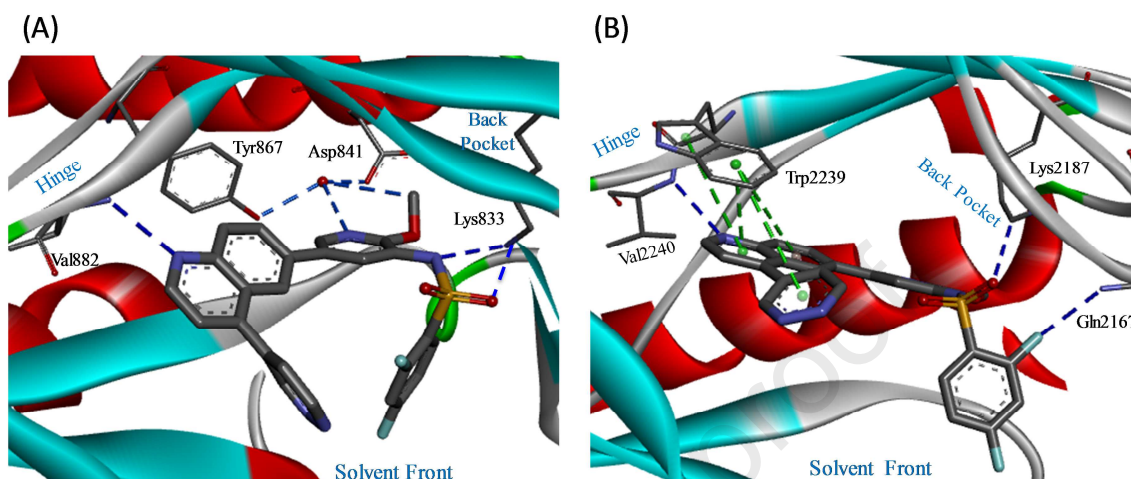


Fig. 1. GSK-2126458. (A) X-ray co-crystal structure of PI3K- γ with GSK-2126458 (PDB 3L08). (B) Docking of GSK-2126458 in mTOR from PDB 4JSX (crystal structure of mTOR-Torin 2 complex from Ref. 14). Dash blue lines highlight hydrogen bond interactions, and dashed green lines represent Pi-interactions.

Based on this information, we designed a series of MCXs using the quinoline core present in GSK-2126458, and alternative bicyclic scaffolds that hold the acceptor N in a similar position. Several aryl, heteroaryl and heterocycloalkyl moieties were used as substituents of these scaffolds, and connected to the 2,4-diF-Phenyl (or Ph) group *via* amide linkers to obtain the corresponding macrocyclic derivatives (Fig. 2).

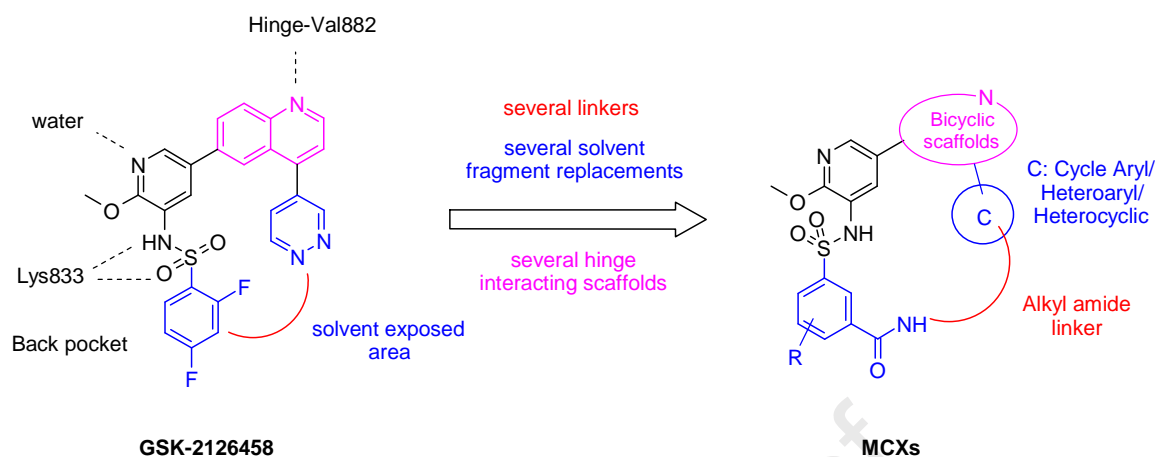
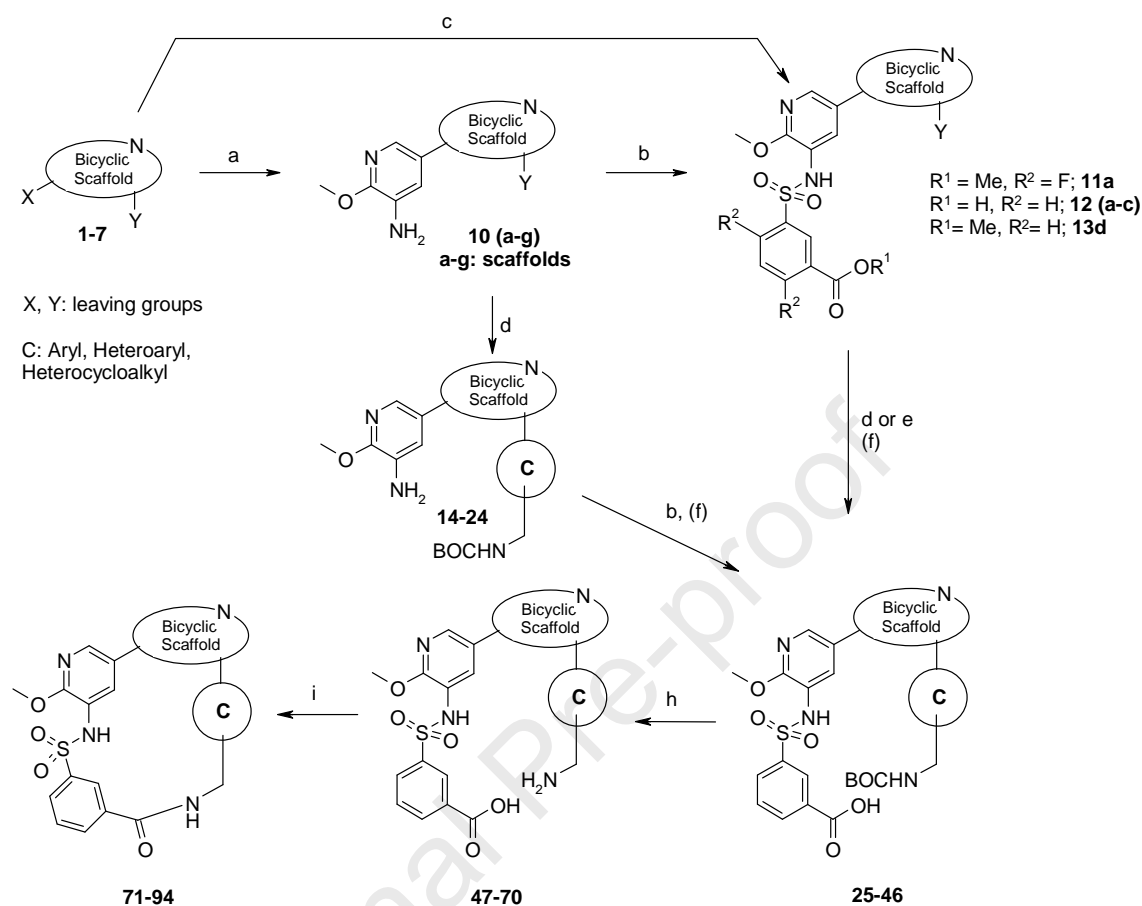


Fig. 2. Macrocyclic series design. Schematic representation of key interactions of GSK-2126458 in PI3K- γ . General structure of resulting MCXs.

2.2. Chemistry

The synthetic strategy to prepare the designed MCXs and the necessary intermediates is depicted in Schemes 1 and 2.



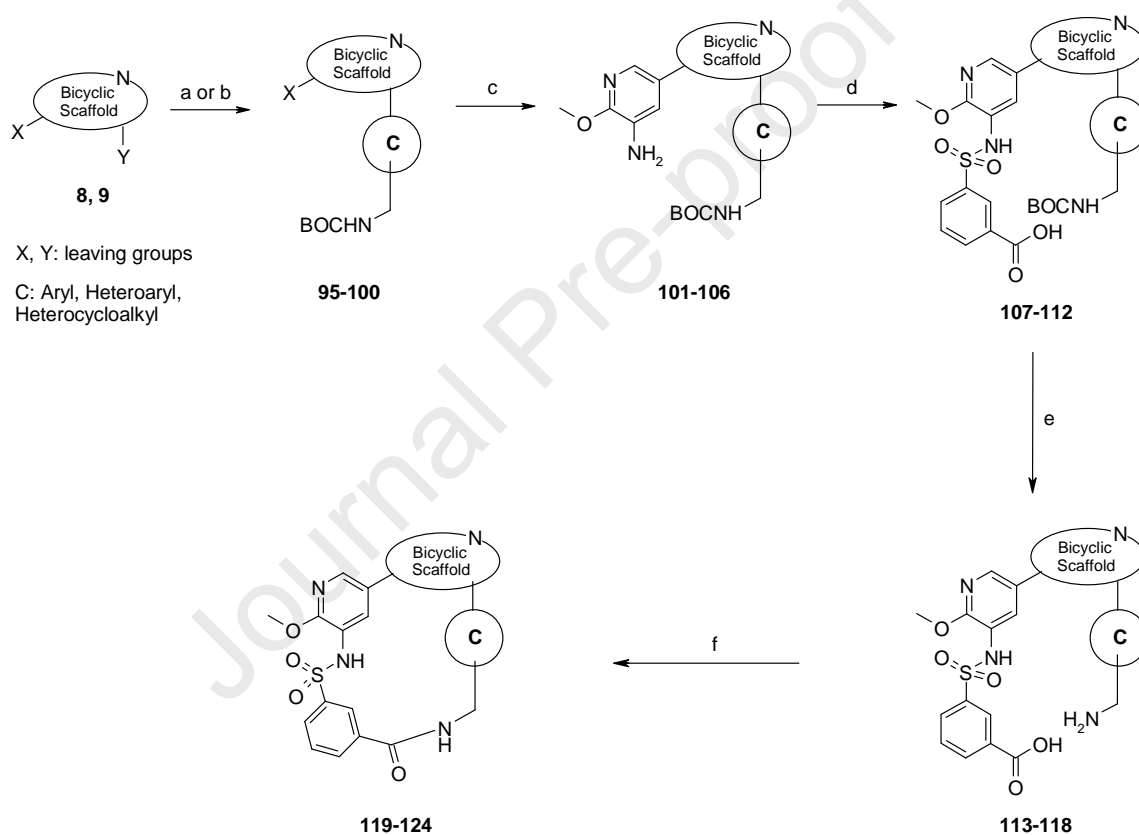
Scheme 1. Synthesis of MCXs **71-94**. Reagents and conditions: (a) (5-Amino-6-methoxypyridin-3-yl)boronic acid pinacol ester, $\text{Pd}(\text{PPh}_3)_4$ or $\text{Pd}(\text{dppf})\text{Cl}_2$ or $\text{PdCl}_2(\text{PPh}_3)_2$, K_2CO_3 or Na_2CO_3 in H_2O , dioxane or DME, $80\text{ }^\circ\text{C}$ - $110\text{ }^\circ\text{C}$. (b) Benzenesulfonyl chloride reagents, pyridine. (c) Boronic acid of [2-methoxy-pyridin-3-ylsulfamoyl]-benzoic acid methyl ester, $\text{Pd}(\text{PPh}_3)_4$ or $\text{PdCl}_2(\text{PPh}_3)_2$, K_2CO_3 or Na_2CO_3 in H_2O , dioxane or DME, $80\text{ }^\circ\text{C}$ - $100\text{ }^\circ\text{C}$. (d) Ar/Heteroaryl boronic acid derivatives, $\text{Pd}(\text{PPh}_3)_4$ or $\text{PdCl}_2(\text{PPh}_3)_2$ or $\text{Pd}(\text{dba})_2/\text{Ph}_3\text{P}$, K_2CO_3 or Na_2CO_3 in H_2O , dioxane or DME, $80\text{ }^\circ\text{C}$ - $115\text{ }^\circ\text{C}$ or $110\text{ }^\circ\text{C}$ - $150\text{ }^\circ\text{C}$ under microwave irradiation. (e) Heterocyclic amines, NMP, $150\text{ }^\circ\text{C}$. (f) $\text{LiOH}\cdot\text{H}_2\text{O}$ in MeOH or K_2CO_3 in dioxane at $110\text{ }^\circ\text{C}$. (h) TFA-DCM or HCl 4N in dioxane. (i) DIPEA,

PyBOP/DMAP or HATU/HOAt as coupling agents, DMF high dilution. List of MCXs in Tables 1, 2.

The syntheses of MCXs were accomplished starting from the commercial available functionalized bicycles **1-9**: 6-bromo-4-chloroquinoline (**1**), trifluoro-methanesulfonic acid 8-chloro-[1,5]naphthyridin-2-yl ester (**2**), 4-chloro-6-iodo-thieno[2,3-*d*]pyrimidine (**3**), 4-chloro-2-iodo-1H-pyrrolo[2,3-*b*]pyridine (**4**), 3-bromo-6-iodoimidazo[1,2-*a*]pyridine (**5**), 3-bromo-5-chloro-pyrazolo[1,5-*a*]pyrimidine (**6**), 2-bromo-5-iodo-imidazo[2,1-*b*][1,3,4]thiadiazole (**7**), 6-bromo-4-chloro-quinazoline (**8**), and 3-bromo-6-chloro-imidazo[1,2-*b*]pyridazine (**9**). Compounds **1-7** reacted, according to Scheme 1, with (5-amino-6-methoxypyridin-3-yl) boronic acid pinacol ester under palladium-catalyzed coupling conditions to give their respective intermediates **10 (a-g)**. Next, we were able to obtain compounds **25-46** following a sequence of two consecutive steps that can be inverted: first, sulfonylation of the amino group of the 2-methoxypyridinyl fragment of **10**, and then introduction of the aryl/heteroaryl/heterocyclic (C) moiety; or on the other way around. Thus, using the appropriate substituted benzenesulfonyl chlorides in dry pyridine as solvent we obtained the corresponding sulfonamides derivatives **11-13**, which further reacted with different aryl/heteroaryl boronic/boronates *via* palladium-catalyzed coupling or with excess of heterocyclic amines by nucleophilic substitution. The reverse sequence of reactions involved first the Suzuki palladium coupling of **10** with different boronic/boronates to give intermediates **14-24**, which later reacted with the corresponding benzenesulfonyl chloride reagents to form the expected compounds. An additional ester basic hydrolysis step was required for those compounds that contained this group.

Boc group deprotection of **25-46** under acidic conditions afforded key precursors **47-70** that rendered final macrocyclic compounds (**71-94**) by classical amide formation reactions under high dilution conditions to favor the desired macrocyclization.

The synthesis of MCXs **119-124** derived from 6-bromo-4-chloro-quinazoline (**8**) and 3-bromo-6-chloro-imidazo[1,2-*b*]pyridazine (**9**) followed the conditions described in Scheme 2.



Scheme 2. Synthesis of MCXs **119-124**. Reagents and conditions: (a) Aryl/Heteroaryl boronic acids derivatives, Pd(PPh₃)₄ or Pd(dppf)Cl₂ or PdCl₂(PPh₃)₂, K₂CO₃ or Na₂CO₃ in H₂O, dioxane or DME, 80 °C-100 °C or 120 °C-140 °C under microwave irradiation. (b) Heterocyclic amines, TEA, DCE, 0 °C to rt. (c) (5-Amino-6-methoxypyridin-3-yl)boronic acid pinacol ester, Pd(PPh₃)₄ or Pd(dppf)Cl₂ or PdCl₂(PPh₃)₂, K₂CO₃ or Na₂CO₃ in H₂O,

dioxane or DME, 80 °C-120 °C. (d) 3-(Chlorosulfonyl)benzoic acid, pyridine, 0 °C and rt. (e) TFA, DCM. (f) DIPEA, HATU, HOAt, DMF high dilution. See structure and numbering of compounds in Table 2.

Reaction of functionalized bicycles **8** at C-4, and **9** at C-3 position with different aryl/heteroaryl boronic acid derivatives or with heterocyclic amines at the indicated conditions rendered compounds **95-100**. Then, Suzuki coupling reaction was used to insert the 5-amino-6-methoxypyridin-3-yl moiety affording **101-106**. Subsequent sulfonylation with 3-(chlorosulfonyl)benzoic acid in pyridine yielded compounds **107-112**, which were transformed into the corresponding “amino/acid” intermediates **113-118** after BOC-deprotection under acidic conditions. The final amide macrocyclization reactions, following conditions described above rendered desired MCXs **119-124**.

2.2. Biological evaluation.

2.2.1. Biochemical activity

We evaluated in dose response experiments the inhibitory activity of the prepared MCXs against PI3K- α and mTOR (IC_{50} value, half-maximal inhibitory concentration) [15]. In general, we obtained highly potent biochemical PI3K- α /mTOR inhibitors with IC_{50} values within the low nanomolar and even picomolar range (Tables 1, 2), and different inhibition ratios for both kinases under these experimental conditions.

GSK-2126458 was reported as a strong dual inhibitor with slight preference for PI3K- α vs. mTOR [13]. This dual activity was also observed under our experimental conditions (PI3K α IC_{50} = 1.0 nM; mTOR IC_{50} = 1.2 nM). The quinoline based MCXs (Table 1) showed

good PI3K- α activity in the range of 0.8-23.2 nM, being the most active the MCX **71**, bearing 3-pyridinyl and di-F-phenylsulfonamide fragments. The removal of both F atoms (**72**) led to a subtle change of activity (\sim 2-fold; $IC_{50} = 2.0$ nM). The replacement of the 3-pyridine by a Ph group (**77**) yielded a \sim 6-fold less potent MCX although retained a still potent activity of 6.1 nM. The corresponding de-fluorinated analogue (**79**) showed similar drop of activity observed between MCXs **71** and **72**. Noteworthy, the exchange of 3-pyridine by the 4-pyridine regioisomer produced a 10-fold decrease of PI3K- α activity (**72** vs. **80**). The introduction of a 3-pyrazole moiety together with an additional methylene group in the linker gave a potent MCX (**76**, $IC_{50} = 4.6$ nM), and comparable to the 3-pyridine analogue **72**. Interestingly, the *ortho*-fluorinated phenyl linker analogues of **79**, MCXs **75** and **81**, yielded opposite outcome in terms of PI3K- α activity. Thus, the “2-F-5-substituted analogue” (**75**) resulted to be slightly more potent ($IC_{50} = 3.8$ nM) whereas the “2-F-3-substituted derivative” (**81**) decreased its activity ($IC_{50} = 23.2$ nM) with respect to **79**. Furthermore, the replacement of the benzylamine portion of the linker in **79** by a tetrahydroisoquinoline fragment (**73**) afforded a more potent PI3K- α inhibitor ($IC_{50} = 2.2$ nM), and demonstrated that the NH of the amide group in the linker was expendable to obtain potent activity. Importantly, those MCXs with heterocycloalkyl linkers such as piperidine **74** and **78** were also active ($IC_{50} = 2.9$ nM and 11.5 nM) suggesting that additional chemical diversity in the linker region of these molecules was compatible with PI3K- α activity.

MCXs **71-81** displayed diverse inhibitory activity against mTOR, ranging from 0.3 nM to 655 nM. The most potent MCX was **73** ($IC_{50} = 0.3$ nM) followed by **74** ($IC_{50} = 4.1$ nM), both with a tertiary amide linker in their structure. Noteworthy, MCX **78**, the NH analogue

of **74**, was 18-fold less potent ($IC_{50} = 72.2$ nM) pointing to a beneficial effect of the N-Methylation of this linker to gain mTOR activity. 3-pyrazole- (**76**, $IC_{50} = 20.9$ nM) and 3-pyridyl- linkers (**71** and **72**, $IC_{50} = 22.3$ and 63.8 nM) were well accommodated in the binding site of mTOR. The comparison of MCXs **71** and **72** demonstrated the positive influence of the fluorine atoms of the phenylsulfonamide ring for mTOR potency. This effect was already observed for the inhibition of PI3K- α . The better mTOR activity of MCX **77** over **79** further supported this trend ($IC_{50} = 122$ vs. 655 nM). The “fluorine effect” was also observed in the F-substitution of the Ph-linker of **79**. This modification was able to recover mTOR potency in MCXs **75** and **81** ($IC_{50} \sim 250$ nM). Finally, the 4-pyridil linker of MCX **80** ($IC_{50} \sim 250$ nM) led to a similar improvement mTOR activity with respect to the Ph-linker analogue **79**.

From this exploration, we concluded that some of our MCXs displayed potent dual PI3K/mTOR inhibition (**74**, **76**), whereas others (e.g. **71**, **72**, **75**, and **77**) were more PI3K- α selective inhibitors (mTOR/PI3K- α ratio ≥ 20). Interestingly, the tetrahydroisoquinoline linker MCX **73** behaved as a strong dual inhibitor with preference for mTOR (mTOR/PI3K- α ratio = 0.13).

The interpretation of the observed SAR in Table 1, and in Table 2 where other scaffolds have been explored, could be rather speculative, unless a detailed computational study and/or generation of X-ray co-crystal structures is achieved [16]. These studies, out of the scope of the current work, are underway and their results will be reported in due course. However, preliminary docking studies have been performed with one of our selected compounds, MCX **83**, confirming a similar binding mode than Omipalisib (Fig. 6).

The SAR interpretation for MCXs is often complex and less straightforward than for “open small molecules”. The coupling of bond rotations and intramolecular interactions enables the transmission of three-dimensional information from one side of a MCX to the other. On other words, making relatively small structural modifications to a MCX can result in local conformational changes that propagate along the ring to affect distal structural features [17]. Thus, modifications of the (C)-substituent (linkers), and scaffolds in our MCXs could lead to distinct preferred conformations and affect their binding in PI3K and/or mTOR, reinforcing or weakening key interactions in an unexpected manner. Comparatively, the SAR for the same modifications in analogous “open small molecules” could be interpreted attending to more local and classical effects of the substituents, well known for medicinal chemists.

Besides the conformational influence of the explored modifications in our MCXs, we can enumerate other factors, which could play (or not) a role to the observed SAR.

1. The structural information available for GSK-2126458 (PDB 3L08) [13], and a related morpholinyl analogue (PDB 3S2A) [18], showed the absence of interactions of the (C)-substituent at C-4 of the quinoline scaffold in the binding site of PI3K- γ , and by homology with PI3K- α .

Additionally, a diverse set of C-4 substituents in this series was tolerated without significant changes in their PI3K activity [18].

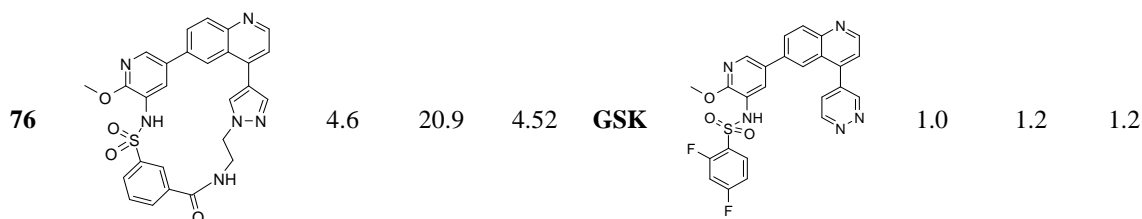
2. The (C)-substituent at the explored scaffolds could affect their acceptor capacity to establish H-bond interactions with Val851/Val2240 in PI3K- α /mTOR. As well, the intrinsic capacity of the explored bicyclic scaffolds to interact with these key residues should be taken into account.

3. The contribution of the different MCXs (mainly the scaffolds) to achieve more or less productive pi-stacking interactions with Trp2239 in the binding site of mTOR should be considered to further rationalize the SAR observed against this kinase.

Table 1

IC₅₀s (nM)^a of PI3K- α , mTOR, and mTOR/PI3K- α ratios.

Nr	Structure	PI3K	mTOR	ratio	Nr	Structure	PI3K	mTOR	ratio
71		0.8	22.3	27.8	77		6.1	122	20.3
72		2	63.8	31.7	78		11.5	72.2	6.3
73		2.2	0.3	0.13	79		13.4	655	48.9
74		2.9	4.1	1.41	80		20	223	11.1
75		3.8	250	65.9	81		23.2	249	10.7



^aThe reported values are the average of two independent data points. PI3K- α activity was determined using ADP-HunterTM Plus, and mTOR with LanthaScreenTM assay.

GSK, GSK-2126458.

We explored alternative scaffolds, bearing the required acceptor N atom, to establish key H-bond interactions with Val851 in PI3K- α and Val2240 in mTOR. The initial quinoline scaffold was replaced by 1,5-naphthyridine (**82-84**), thieno[2,3-*d*]pyrimidine (**85-86**), 1H-pyrrolo[2,3-*b*]pyridine (**87**), imidazo[1,2-*a*]pyridine (**88-89**), pyrazolo[1,5-*a*]pyrimidine (**90-92**), imidazo[2,1-*b*][1,3,4]thiadiazole (**93-94**), quinazoline (**119-122**) and imidazo[1,2-*b*]pyridazine (**123-124**). The linkers for this exploration were selected from those used for the quinoline MCXs. The compounds were synthesized following the general procedure depicted in Scheme 1 and 2. MCXs (**82-124**) were tested against PI3K- α and mTOR kinases yielding the results summarized in Table 2.

The quinazoline MCXs **119-122** were potent PI3K- α inhibitors showing IC₅₀ values below 3.0 nM. The comparison with their corresponding quinoline pairs afforded similar or even better PI3K- α activity for the quinazolines series (~5-fold for **119**, **121**, and **122**). The mTOR inhibition was improved between 3 to 20-fold in all the MCXs in comparison with their quinoline analogues.

The replacement of the quinoline ring by 1,5-naphthyridine afforded highly potent dual inhibitors (**82-84**). The improvement of mTOR activity within this series was significant in

comparison with quinoline analogues. Thus, MCX **82** achieved a 40-fold increase in potency *vs.* analogue **79** ($IC_{50} = 16.5$ *vs.* 655 nM). Once again, the presence of fluorine atoms in the phenylsulfonamide fragment (**83**) improved both PI3K- α and mTOR activities ($IC_{50} = 0.8$ and 3.3 nM) *vs.* phenylsulfonamide analogue **84** ($IC_{50} = 3.7$ and 23.4 nM).

The improvement of mTOR activity of quinazoline and 1,5-naphthyridine MCXs might be highly related to the establishment of more favorable π -stacking interactions of these more electron deficient scaffolds with Trp2239 side chain, among other factors cited above.

Next, we explored thieno[2,3-*d*]pyrimidine MCXs **85** and **86**. This scaffold reduced the PI3K- α potency of these MCXs in comparison with their quinazoline analogues, although MCX **85** still showed an interesting activity ($IC_{50} = 20.4$ nM). Similar results were reported for a pair of non-macrocyclic inhibitors, where the thieno[2,3-*d*]pyrimidine scaffold produced a ~ 20 -fold decrease in PI3K- α activity when compared to the corresponding quinazoline analogue [19]. The argument to explain such decrease in activity was the possible lone pair repulsion between the sulfur in the thienopyrimidine core and the backbone carbonyl oxygen of Glu880 in PI3K- γ (surrogate of the homologous PI3K- α). Conversely, other general reports could point to a productive σ -hole type interaction between the S atom and the carbonyl oxygen of Glu880 [20]. As alternative, we cannot discard just a less H-bond acceptor character of thienopyrimidine scaffold *vs.* quinazoline to explain the PI3K- α SAR.

The influence of the thienopyrimidine scaffold was much more pronounced in mTOR, yielding nearly inactive MCXs. The reduction of mTOR activity was evident in comparison with quinazoline analogues (**85** *vs.* **119** and **86** *vs.* **120**; $IC_{50} = 5790$ nM *vs.* 30.5 nM, and > 10000 nM *vs.* 16.7 nM).

A potential steric repulsion between the S atom and Tyr2245 was argued to justify a decline in m-TOR activity when a quinazoline scaffold was replaced by thieno[2,3-*d*]pyrimidine in related open analogues [19]. Furthermore, we could also suggest unfavorable pi-stacking interactions of more electron rich thieno[2,3-*d*]pyrimidine scaffold with Trp2239 as contributor for such results, besides other conformational factors cited above.

The 1H-pyrrolo[2,3-*b*]pyridine MCX **87** was designed to get an additional H-bond with the backbone carbonyl group of Glu849 in PI3K- α . Unfortunately, **87** was the weakest inhibitor of PI3K- α in our series ($IC_{50} = 445.0$ nM) and proven to be inactive against mTOR. The poor activity against PI3K- α indicated a negligible formation of the postulated bidentate H-bond, perhaps due to conformational limitations to achieve a good fitting in the binding site of both kinases.

The electron rich character of this scaffold could also be detrimental for the mTOR activity of MCX **87** due to unfavorable interactions with Trp2239.

The exploration of several MCXs using 5-6 bicyclic scaffolds was also achieved. Pyrazolopyrimidine MCXs (**90-92**) gave potent PI3K- α ($IC_{50} < 4.1$ nM) and mTOR inhibitors ($IC_{50} < 40$ nM). Moreover, the structurally similar imidazopyridazine MCXs **123** and **124** afforded again potent PI3K- α inhibition ($IC_{50} \sim 5.0$ nM) although slightly less potent than their direct analogues **91** and **92**. Regarding mTOR, the imidazopyridazine MCXs followed the same trend observed for their pyrazolopyrimidine counterparts. Compound **123** showed a well-balanced PI3K- α and mTOR activity with ratio of 1, and in the case of 3-pyrazole derivative (**124**) the ratio was ~ 14 . The removal of the six membered ring N from the imidazopyridazine scaffold led to the imidazopyridine analogues **88** and

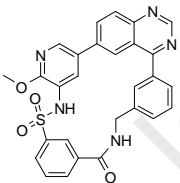
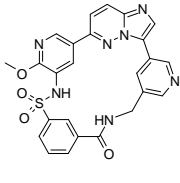
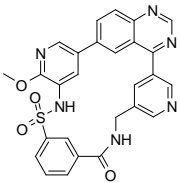
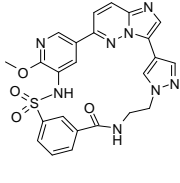
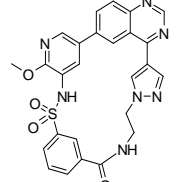
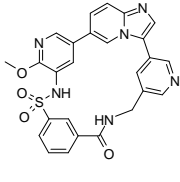
89. Compound **89** showed similar potency against PI3K- α and mTOR than **124**, but MCX **88** was 2.5-fold less potent for PI3K- α , and 9-fold less potent for mTOR than its analogue **123**.

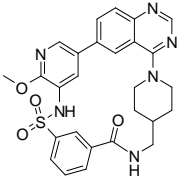
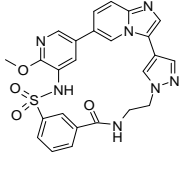
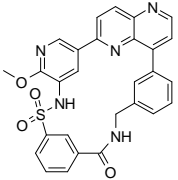
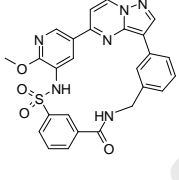
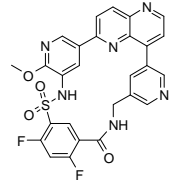
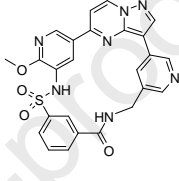
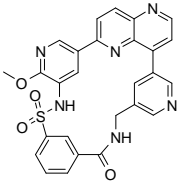
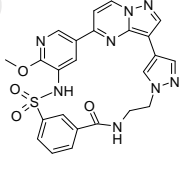
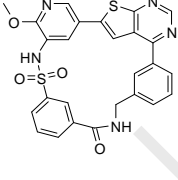
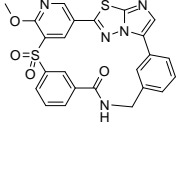
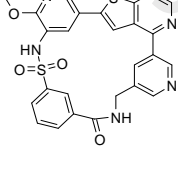
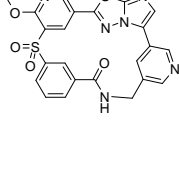
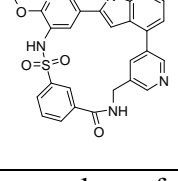
Finally, we explored a 5,5-bicyclic scaffold such as imidazothiadiazole with the corresponding phenyl and 3-pyridine linkers. MCXs **93** and **94** exerted potent PI3K- α inhibition (IC_{50} = 8.9 and 16.2 nM) although their mTOR activity was significantly weaker (IC_{50} = 361 and 1060 nM).

The arguments described to justify previous SAR cases could also be applied for MCXs derived from 5-6 and 5-5 membered rings scaffolds.

Table 2

PI3K- α and mTOR IC_{50} s (nM).^a

Nr	Structure	PI3K	mTOR	ratio	Nr	Structure	PI3K	mTOR	ratio
119		2.5	30.5	12.3	123		4.6	5.4	1.2
120		3.0	16.7	5.5	124		5.0	67.6	13.6
121		1.3	4.9	3.8	88		11.5	49	4.3

122		2.1	5.6	2.7	89		7.7	66.3	8.7
82		5.0	16.5	3.3	90		2.9	4.7	1.6
83		0.8	3.3	4.1	91		1.0	4.4	4.6
84		3.7	23.4	6.3	92		4.1	39.9	9.6
85		20.4	5790	284	93		8.9	361	40.4
86		85.3	>10000	>117	94		16.2	1060	65.4
87		445	>10000	>22					

^a Average values of two independent experiments. PI3K- α activity was determined using ADP-HunterTM Plus, and mTOR with LanthaScreenTM assay.

Several conclusions were extracted from the exploration described in Table 2. Most of the MCXs displayed potent PI3K- α inhibition ($IC_{50} < 20$ nM), except those with thienopyrimidine and pyrrolopyridine scaffolds. The different linkers explored in potent MCXs inhibitors did not afford drastic changes in PI3K- α activity (< 10 -fold with IC_{50} values in the low or sub-nanomolar range). It was observed a more pronounced inhibition of PI3K- α than mTOR along the explored MCXs, although many MCXs could be cataloged as dual PI3K- α /mTOR inhibitors (ratios < 10 , and IC_{50} values in nanomolar range). Conversely, several MCXs were more selective PI3K- α inhibitors than GSK-2126458 (mTOR/PI3K- α ratio of 1.24) such as imidazothiadiazoles **93** and **94** with ratio > 30 , and the thienopyrimidine PI3K- α inhibitor **85** with ratio = 284.

2.2.2. Cellular activity

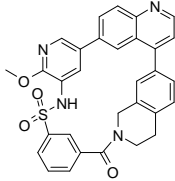
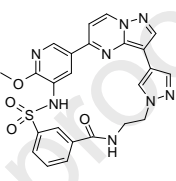
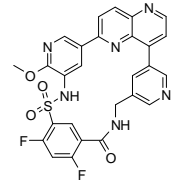
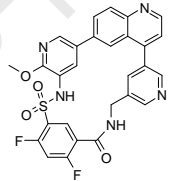
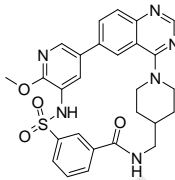
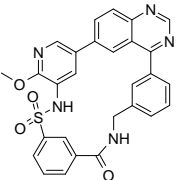
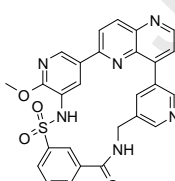
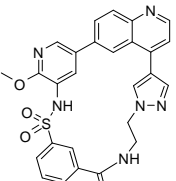
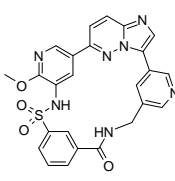
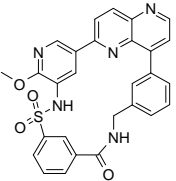
Next, the cellular activity of the compounds with interesting dual biochemical activity (PI3K- α /mTOR IC_{50} values < 10 nM / < 50 nM respectively) was evaluated in U2OS cells by measuring their effects on the phosphorylation of AKT on Ser473. This phosphorylation event is dependent on the orchestrated activities of PI3K, mTORC1, and mTORC2. The inhibition of PI3K inhibits mTORC1 activity, and through a feedback loop mechanism activates mTORC2, the kinase responsible of the AKT phosphorylation on Ser473. Besides, mTORC1 inhibition triggers PI3K activation *via* RTKs modulation. Therefore, the inhibition of p-AKT^{Ser473} is a good measurement of the efficacy of dual PI3K/mTOR inhibitors to control the PI3K/mTOR/AKT signaling pathway.

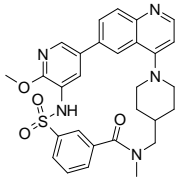
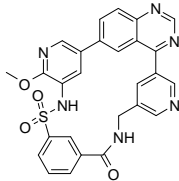
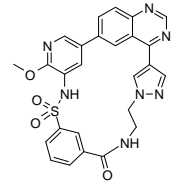
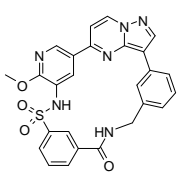
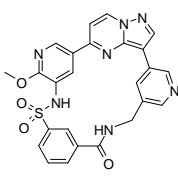
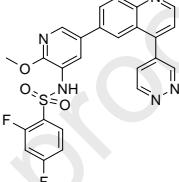
In general, it was observed a good inhibition of p-AKT^{Ser473} with $EC_{50} < 100$ nM for all MCXs, except for the pyrazolopyrimidine **90** (Table 3). The activity of MCXs **73** and **83**

was even better than the reference compound GSK-2126458 under our experimental conditions.

Table 3

Biochemical (IC₅₀) and Cellular activity (p-AKT, EC₅₀) in nM.^a

Nr	Structure	PI3K	mTOR	P ⁻ AKT	Nr	Structure	PI3K	mTOR	P ⁻ AKT
73		2.2	0.3	0.10	92		4.1	39.9	38.9
83		0.8	3.3	0.17	71		0.8	22.3	10.7
122		2.1	5.6	4.58	119		2.5	30.5	47.9
84		3.7	23.4	9.00	76		4.6	20.9	61.9
123		4.6	5.4	10.8	82		5.0	16.5	72.3

74		2.9	4.1	18.3	120		3.0	16.7	99.4
121		1.3	4.9	20.6	90		2.9	4.7	203
91		1.0	4.4	37.1	GSK		1.0	1.2	0.6

^a Average values of two independent experiments.

GSK: GSK-2126458.

2.2.3. ADME-T properties of MCXs

We were intrigued about the potential transference of drug-like properties of our starting point of design, the clinical inhibitor GSK-2126458, to the newly discovered macrocyclic inhibitors. First, the metabolic stability of MCXs with better cellular potency (p-AKT EC₅₀ < 50 nM) was measured using human, mouse and rat liver microsomes. The results are summarized in Table 4.

Table 4

ADME-T data.

Nr	hLM (%) ^a	mLM (%) ^a	rLM (%) ^a	CYP1A2 IC ₅₀ μM	CYP2C19 IC ₅₀ μM	CYP2C9 IC ₅₀ μM	CYP2D6 IC ₅₀ μM	CYP3A4 IC ₅₀ μM
71	89	88	97	>30	>30	8.3	>30	>30

73	69	57	63	>30	14.7	3.1	>30	19.6
74	79	64	72	>30	>30	>30	>30	>30
83	100	97	100	>30	>30	>30	>30	>30
84	77	77	75	>30	>30	>30	>30	>30
91	90	85	92	>30	>30	>30	9.9	>30
92	66	61	57	>30	>30	>30	>30	>30
119	97	74	91	>30	>30	>30	>30	>30
121	80	76	86	>30	>30	>30	>30	>30
122	74	63	70	>30	16.8	0.9	>30	>30
123	93	63	90	>30	19.7	6.5	>30	6.5

^a Percentage of compound remaining after 15 min incubation in human, mouse and rat liver microsomes.

In general, the tested MCXs were rather metabolically stable displaying high levels of intact parent compounds after 15 minutes of incubation. The main exceptions were the quinoline MCX with a tetrahydroisoquinoline linker **73** and the pyrazolopyrimidine MCX **92** bearing a pyrazole linker, which showed weaker stability in all species (~ 60% of compound remaining).

It is well known that combinatorial therapy is widely used in cancer treatments. In order to be safe in these therapeutic scenarios a drug should be free of potential drug-drug interactions. CYP450 inhibition has been identified as a major source for drug-drug interactions in combinatorial therapy [21]. Therefore, we tested the inhibitory activity of our MCXs in a panel of CYP450 enzymes (Table 4). All compounds displayed excellent profiles with negligible inhibition of the CYP450 enzymes or ample therapeutic windows

against their primary activity. The exception was MCX **122** which showed significant inhibition of CYP2C9 with IC_{50} below 1 μ M.

The blockage of the human “Ether-à-go-go-Related Gene” channel (h-ERG) is associated with cardiotoxicity since it can lead to a heart related fatal disorder called “Long QT syndrome”. It is characterized by ventricular arrhythmias, particularly torsades de pointes (TdP) [22]. The early detection of this liability within drug discovery programmes is crucial to progress drug candidates towards the clinic. We tested the binding of our MCXs against h-ERG, and none of them displayed significant binding ($IC_{50} > 30 \mu$ M).

2.2.4. *In vivo* Pharmacokinetics

We assessed the pharmacokinetic properties of selected MCXs in BALB-C mice after I.V. and P.O. administration. We selected some dual PI3K/mTOR inhibitors based on potency, cellular activity (p -AKT $EC_{50} \leq 20$ nM), microsomal stability higher than 75% in all species tested, and without any significant ADME-T alert. Compound **73** was also included due to its picomolar cellular activity. These compounds are representatives of three different scaffolds. The results of these studies are summarized in Table 5. The tested MCXs showed oral bioavailability with F_{abs} ranging from 27% to 85%. The *in vivo* clearance (Cl) was below 10% of mouse hepatic blood flow rate for all MCXs (Cl: 0.22-0.56 L/h/Kg) except for **83**, with moderate values (Cl= 1.89 L/h/Kg; 35% of hepatic blood flow). The volume of distribution (Vd) was moderate for the compounds with low clearance (0.28-0.59 L/Kg; accounting for 47-98% of the total body water content of the animals), indicating that the compounds are increasingly distributed in total body compartments. By contrast, MCX **83** showed higher Vd (5.98 L/Kg) suggesting much

higher distribution in peripheral tissues, which could be relevant in the treatment of solid tumors. In this regard, the volume of distribution reported for GSK-2126458 (Table S1) was of 1 L/Kg [13].

Table 5

Pharmacokinetic (PK) profile.^a

Nr	I.V.					P.O.					
	Dose	AUC _{inf}	T _{1/2}	Cl	Vd	Dose	C _{max}	T _{max}	T _{1/2}	AUC _{inf}	F %
71	5	9467.6	0.57	0.53	0.28	10	3389.3	0.25	2.78	7681	40.6
73	1	4455.1	2.01	0.22	0.58	3	962.3	0.50	3.35	3648	27.3
83	5	2644.4	2.59	1.89	5.98	10	1565.8	0.50	5.22	4475	84.6
84	5	8930.8	0.99	0.56	0.41	10	1635.2	0.25	1.81	5029	28,2
121	5	9203.9	2.91	0.54	0.59	10	1266.3	0.16	5.68	8761	47.6

^a PK studies performed I.V./P.O. at the indicated doses during 8 h. The data were adjusted to a non-compartmental model using Winnolin software. Units of PK parameters: Dose (mg/Kg); Area Under Curve AUC (h.ng/ml); half life T_{1/2} (h); Clearance Cl (L/h/Kg); Volume of distribution Vd (L/ Kg); Maximum concentration C_{max} (ng/ml). Time of maximum concentration T_{max} (h).

All MCXs showed good oral exposures and achieved plasma concentrations (measured up to 8 h) that fairly exceeded the EC₅₀ values for inhibition of p-AKT^{Ser473} in cells (Fig. 3). The best ratios were observed for MCXs **73** (3 mg/Kg dose) followed by **83** (10 mg/Kg dose) mainly due to their high cellular activity (Fig. 3).

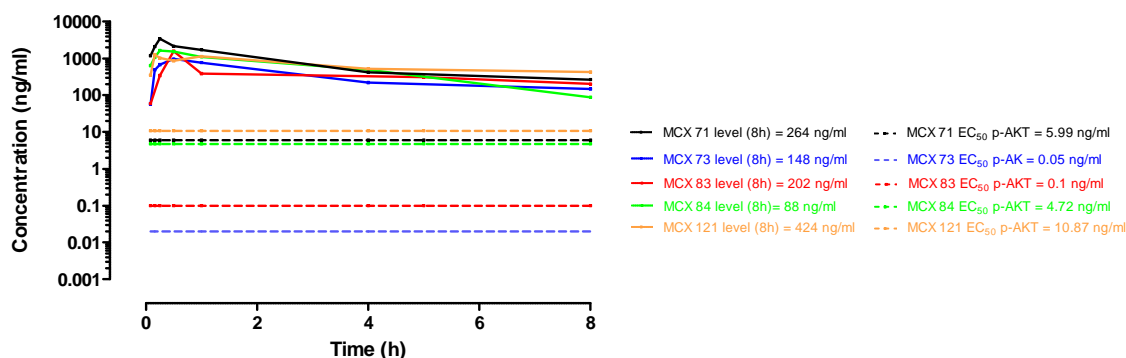


Fig.3. PK profiles after PO administration. The solid lines represent plasma compound levels and dashed lines represent their EC_{50} values for inhibition of p-AKT^{Ser473} in U2OS cells.

The profile of our MCXs indicated oral exposures able to achieve *in vivo* activity at the doses tested, while ensuring a good elimination rate to avoid excessive accumulation of compounds after repeating dosing (half-lives ranged from 1.8 h to 5.7 h). Therefore, the described dual MCX PI3K/mTOR inhibitors qualified as candidates for further *in vivo* antitumoral efficacy studies in mice.

2.3. Additional characterization of compound 83

Among the set of compound characterized in *in vivo* PK, we selected MCX 83 as an example of a balanced PI3K/mTOR dual inhibitor displaying higher potency for PI3K than for mTOR. This is in agreement with the suggested preferred profile for a dual PI3K/mTOR to block pathway reactivation feedback loops [23].

2.3.1. Kinase selectivity of compound 83

It was screened against a panel of 468 kinases at 1 μ M (KINOMEscan® assay platform). MCX **83** demonstrated outstanding selectivity profile with selectivity score $S(35)$ of 0.025 [24]. MCX **83** exhibited < 35% of the signal produced by the untreated controls only for their expected targets PI3-kinases and mutants (0% signal *versus* control), mTOR (1%) and the related lipid kinase PIP4K2C (Fig. 4, Table S2).

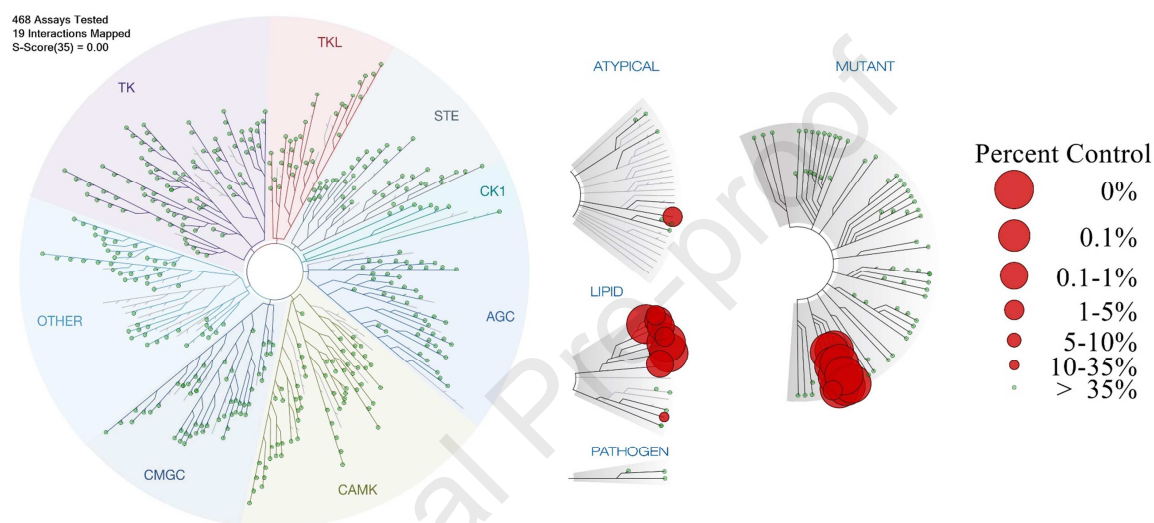


Fig. 4. Selectivity profile of compound **83**. Image generated using TREEspot™ Software Tool and reprinted with permission from KINOMEscan®, a division of DiscoverRx Corporation, © DISCOVERX CORPORATION 2010.

In comparison with MCX **83**, the number of off-targets of GSK-2126458 (KINOMEscan® at 10 μ M) was higher. It could point to a better selectivity of our compound or be just due to the 10-fold higher concentration used in these experiments for GSK-2126458 (Table S3). Nevertheless, we consider that both compounds behave as highly selective PI3K/mTOR inhibitors.

2.3.2. PI3K isoforms and mutants activity

GSK-2126458 is a pan-PI3K inhibitor being active against the catalytic subunits of the PI3K isoforms p110 α , β , δ and γ [13]. We profiled compound **83** against the different

isoforms determining the corresponding K_i values using a high sensitive HTRF based assay by applying the Cheng-Pursoff equation to the experimental IC_{50} values [25, 26]. The results are summarized in Table 6. MCX **83** behaved as pan-PI3K inhibitor attending to the low nanomolar potency against the different isoforms and showed a profile similar to GSK-2126458.

Table 6

K_i values (nM) and ratios among PI3K isoforms.

Nr	PI3K- α	PI3K- β	PI3K- δ	PI3K- γ	Ratio β/α	Ratio δ/α	Ratio γ/α
83	0.16	0.94	0.06	0.98	6.0	0.4	6.3
GSK	0.06	0.53	0.07	0.51	8.8	1.2	8.5

GSK, GSK-2126458

Furthermore, we determined the activity of compound **83** against the common activating mutants of p110 α (E542K, E545K, and H1047R) found in human cancer. MCX **83** was able to inhibit them in the picomolar range (K_i = 0.27, 0.14 and 0.10 nM respectively).

2.3.3. Modulation of PI3K/mTOR activity in cells by MCX **83**

We further validated the effects of MCX **83** on PI3K/mTOR signaling pathways. We treated MCF-7 (breast carcinoma) cell line with different doses of **83** for 3 h, and we measured the inhibition of phosphorylation of different substrates at different level of the pathway. As shown in Figure 5, phosphorylated levels of the PI3K and mTORC2 downstream target, AKT^{S473} were reduced (EC_{50} = 0.46 nM). Phosphorylation of AKT^{T308}, mediated by PDK1 that is activated by PI3K, was also reduced (EC_{50} = 0.14 nM). On the

other hand, inhibition of phosphorylation of mTOR signaling effectors, P70S6K and S6, was observed with EC₅₀s in the low nanomolar range (EC₅₀ = 0.92 and 0.84 nM respectively). The results obtained with GSK-2126458 assayed in the same conditions were rather similar to those of MCX **83** demonstrating that both compounds were potent dual PI3K/mTOR inhibitors (Fig. 5).

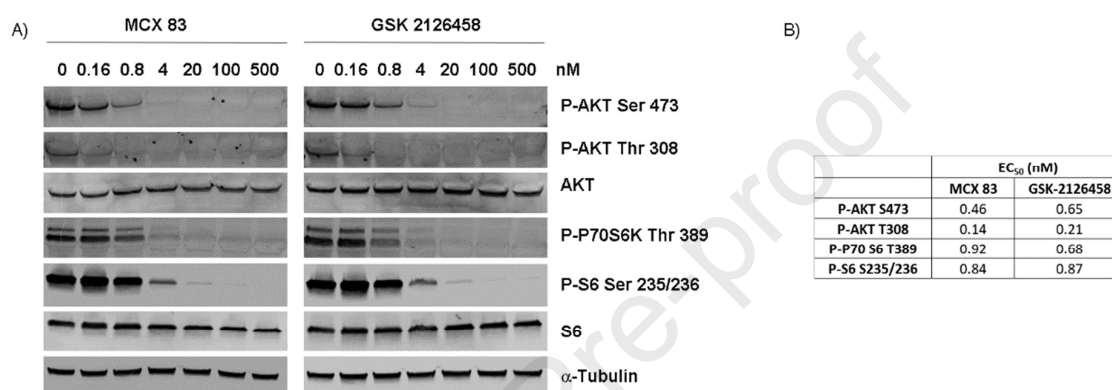


Fig. 5. PI3K/mTOR biomarkers modulation by MCX **83** and GSK-2126458. A) Evaluated by western blot. B) EC₅₀ values.

2.3.4. Evaluation of antiproliferative effects by MCX **83** in tumoral cell lines

MCX **83** was tested for antiproliferative activity *in cellulo* on a series of 14 human cancer lines with mutated p110 α , inactivated PTEN, or p110 α and PTEN wild type (Table 7): breast cancer (MCF-7, BT-549), prostate cancer (DU-145, PC-3), colon (HT-29, HCT-116), non small cell lung carcinoma (A-549, NCI H-1975), renal carcinoma (768-O), ovarian cancer (SK-OV-3), osteosarcoma (U2OS), glioma (U87MG), and leukemia (K562, MOLT-4) using the Cell-Titer Glo® viability assay. MCX **83** demonstrated nanomolar antiproliferative activities with Growth inhibition 50 (GI₅₀) values below 200 nM across the 14 cancer cell lines tested, with a general trend of better values in those cell lines with

mutated p110 α . On the other hand, the antiproliferative activity of GSK-2126458 against selected cell lines was comparable to MCX **83** (Table 7).

Table 7

Growth Inhibition 50 (GI₅₀).

Cell line profile	Cell line	MCX 83 GI ₅₀ (nM) ^a	GSK-2126458 GI ₅₀ (nM) ^a
mutated p110 α	HT-29	8.2 ± 1.7	19.9 ± 1.7
	HCT-116	22.8 ± 6.1	
	MCF-7	7.0 ± 0.9	
	SK-OV-3	18.9 ± 6.6	
	NCI H-1975	4.2 ± 1.1	14.4 ± 1.2
PTEN inactivation	MOLT-4	2.5 ± 1.1	
	U87MG	98.9 ± 22.8	
	768-O	31.9 ± 11.7	
	PC-3	166.5 ± 34.83	197 ± 66.9
Wild type p110 α and PTEN	BT-549	36.1 ± 7.3	
	DU-145	32.7 ± 17.1	16.3 ± 6.6
	K562	139.7 ± 39.5	
	A-549	6.1 ± 2.3	26.6 ± 4.3
	U2OS	78.52 ± 20.9	

^a Mean and sd. of 3 independent experiments.

2.3.5. Molecular docking study for MCX **83**

The docking of MCX **83** in PI3K and mTOR revealed a similar binding mode in the hinge area and the affinity pocket of both kinases (Fig. 6), and comparable to GSK-2126458 (Fig. 1). The naphthyridine scaffold of **83** established interaction with Val882 in the hinge area of PI3K- γ . Additionally, the “pyridosulfonamide” moiety filled the affinity pocket and produced strong electrostatic and H-bonding interactions with Lys833.

Furthermore, the pyridyl N participated in a water bridge with Asp841/Tyr867. On the other hand, one of the sulphonamide O atoms engaged a water molecule to establish a network of interactions with the backbone of residues Lys807/808 and Ser806 side chain. The 4-F of the phenylsulfonamide moiety established an H-bond with Ans951 side chain. The proposed binding mode of MCX **83** predicted another H-bond between the amide C=O group of the linker with the hydroxyl of Ser806 side chain. This interaction might contribute to the observed bending of the P-loop upon MCX **83** binding in comparison with GSK-2126458 co-crystal structure 3L08 (Fig. S1A).

Regarding mTOR, the di-F-phenylsulfonamide fragment in the binding conformation of MCX **83** was less twisted in comparison with the PI3K pose and the N atom of 3-pyridyl moiety pointed down with respect to the central scaffold. The naphthyridine scaffold of MCX **83** established contacts with the hinge region in a similar manner to GSK-2126458, showing a key interaction with Val2240 and pi-stacking with the Trp2239. The “pyridosulfonamide” moiety filled the back pocket area, and established interactions with residues such as Lys2187 and the backbone of Asp2357. The 4-F of the phenylsulfonamide fragment interacted with Ser2165 side chain. Notably, the amide group of the linker did not produce any interaction with mTOR whereas the disubstituted 3-pyridil ring participated in an H-bond with the hydroxyl group of Thr2245. Overall, the comparison of MCX **83** and GSK-2126458 dockings in mTOR did not afford significant structural differences in the protein (Fig. S1B)

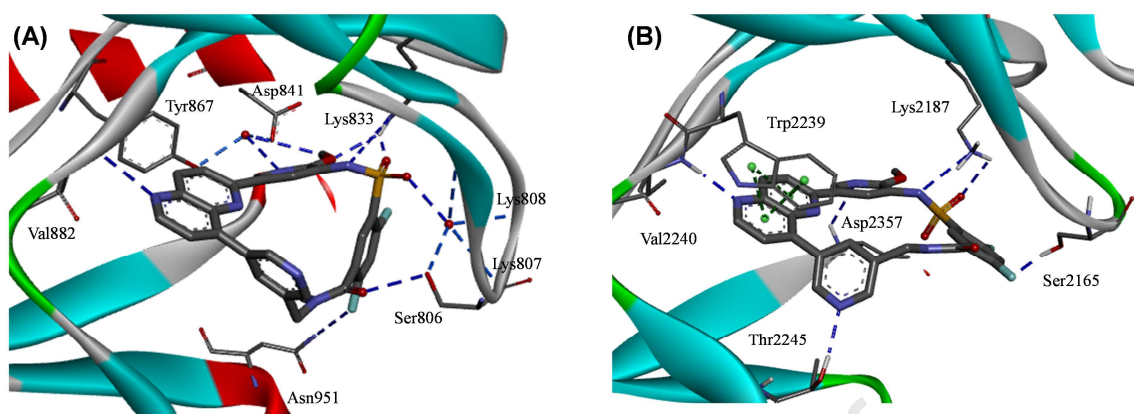


Fig. 6. Docking studies of MCX **83**. (A) in PI3K- γ from PDB 3L08. (B) in mTOR from PDB 4JSX. Dash blue lines highlight hydrogen bond and electrostatic interactions, and dashed green lines represent Pi-interactions.

3. Conclusions

In summary, utilizing a macrocyclization approach starting from the clinical dual PI3K/mTOR inhibitor GSK-2126458 (Omipalisib) we have generated a novel series of MCXs. These molecules are potent dual inhibitors of PI3K/mTOR (even at picomolar level) and fine tune the ratio of inhibition of these oncogenic kinases. Furthermore, the compounds are strong inhibitors of the PI3K/mTOR pathway in cells. Selected MCXs were characterized *in vitro* against several ADME-T properties such as microsomal stability, CYP450 inhibition and h-ERG binding showing promising drug-like properties. Noteworthy, pharmacokinetic studies of selected compounds showed also favorable results. The screening of selected MCX **83** in a panel of 468 kinases yielded an excellent selectivity profile and positioned the compound as candidate for further *in vivo* efficacy studies in animal cancer models. MCX **83** demonstrated to be a pan-PI3K (α , β , δ , γ) inhibitor, and was able to inhibit strongly the oncogenic activating mutants of p110 α (E542K, E545K,

and H1047R). Moreover, MCX **83** potently downregulated cellular phosphorylation of its signaling effectors, and revealed highly potent antiproliferative effects (nanomolar range) in different human tumor cell lines. We believe that these results open a new avenue for the discovery of new potent and selective PI3K/mTOR dual compounds.

4. Experimental

Synthesis of macrocyclic compounds **71**, **73**, **83**, **84** and **121** are described below.

4.1. General Procedures

Chemicals were purchased from Aldrich Chemical Company Ltd., Apollo Scientific Ltd and TCI Europe N.V. unless otherwise stated, commercial chemicals and solvents were used without further purification. Anhydrous DMF, DCM, toluene, MeOH, dioxane, acetonitrile, TEA and DME were purchased from Aldrich in Sure Seal™ bottle and kept under nitrogen. Proton (¹H) NMR spectra were recorded at 300 MHz, Carbon (¹³C) NMR at 75 MHz, and DEPT-135 experiments using Bruker instrument (Bruker Avance II 300) operating at indicated frequencies on using DMSO-*d*₆ or CDCl₃ as solvent. Chemical shifts are expressed in parts per million (ppm) (δ relative to residual solvent peak for ¹H). Multiplicities are indicated by s (singlet), d (doublet), t (triplet), q (quartet), m (multiplet), br (broad) or combination thereof.

The HPLC measurements were performed using a HP 1100 from Agilent Technologies comprising a pump (binary) with degasser, an autosampler, a column oven, a diode-array detector (DAD) and a column Gemini-NX C18 (100 x 2.0 mm; 5 μ m particle size). Eluent A, water with 0.1% formic acid; eluent B: acetonitrile with 0.1% formic acid. Gradient 5% to 100% of B within 8 min at 50 °C, DAD. Flow from the column was split to a MS

spectrometer. The MS detector was configured with an electrospray ionization source or API/APCI. Nitrogen was used as the nebulizer gas. Data acquisition was performed with ChemStation LC/MSD quad. software. Purities of all reported compounds were greater than 95% based on HPLC chromatograms obtained on an Agilent HP 1100 LCMS system. All final compounds were purified to have purity higher than 95% by reverse phase high performance liquid chromatography (HPLC), or normal phase silica gel flash chromatography employing Biotage apparatus (medium pressure liquid chromatography) system SP4 or Isolera™ Prime, using ExtraBond Flash SLL with spacer SI (12 g, 20 g, 40 g, 80 g or 120 g). Thin layer chromatography (TLC) was performed on 20 mm precoated plates of silica gel (Merck, silica gel 60F254); visualization was achieved using ultraviolet light (254 nm). Reactions needing microwave irradiation were carried out in an Initiator Sixty Biotage apparatus (400 W).

4.2. Synthesis of intermediates by Palladium coupling

4.2.1. 5-(4-Chloro-quinolin-6-yl)-2-methoxy-pyridin-3-ylamine (**10a**).

In a sealed tube charged with 4-bromo-6-chloro quinoline **1** (1.0 g, 4.124 mmol) in 1,4-dioxane (33 mL), (5-amino-6-methoxypyridin-3-yl)boronic acid pinacol ester (1.24 g, 4.948 mmol), K₂CO₃ 1M (17 mL) and tetrakis(triphenylphosphine)palladium(0) (482 mg, 0.412 mmol) was heated at 100 °C for 1 h. The reaction mixture was concentrated and purified by column chromatography on silica gel with gradient solvent from 0% to 40% of EtOAc in cHex to give **10a** (864 mg, 73%). LCMS (ESI): Rt = 4.12, m/z =286.2 /288.1 [M+ H]⁺.

4.2.2. 5-(8-Chloro-[1,5]naphthyridin-2-yl)-2-methoxy-pyridin-3-ylamine (**10b**).

The reaction was carried out in two batches of 1.5 g each one. Trifluoro-methanesulfonic acid-8-chloro-[1,5]naphthyridin-2-yl ester **2** (1.5 g, 4.798 mmol), (5-amino-6-

methoxypyridin-3-yl)boronic acid pinacol ester (1 g, 3.998 mmol,) and PdCl₂(PPh₃)₂ (140 mg, 0.200 mmol) were suspended in 1,2-DME (16 mL) and Na₂CO₃ (aq sat sol., 8 mL) was added. The mixture was heated at 80 °C in pressure tube for 30 min. The reaction mixture was concentrated and purified by column chromatography on silica gel with gradient solvent from 0% to 100% of EtOAc in cHex and then gradient from 0% to 20 % of MeOH in EtOAc to give **10b** (1.5 g, 55 %) and a less pure fraction (1.2 g). LCMS (ESI): Rt = 4.03 min, m/z = 287.00 [M+ H]⁺. ¹H NMR (300 MHz, DMSO-*d*₆) δ ppm 8.86 (d, *J* = 4.7 Hz, 1H), 8.50 (d, *J* = 8.9 Hz, 1H), 8.41 (d, *J* = 9.0 Hz, 1H), 8.33 (d, *J* = 2.1 Hz, 1H), 8.02 (d, *J* = 4.8 Hz, 1H), 7.88 (d, *J* = 2.2 Hz, 1H), 3.97 (s, 3H).

4.2.3. *5-[5-(4-Chloro-quinolin-6-yl)-2-methoxy-pyridin-3-ylsulfamoyl]-2,4-difluorobenzoic acid methyl ester (11a).*

To a solution of **10a** (600 mg, 2.10 mmol) in pyridine (8.2 ml) at 0°C was added methyl 5-(chlorosulfonyl)-2,4-difluorobenzoate (682 mg, 2.52 mmol). The mixture was stirred for 2h. The reaction was quenched with MeOH and concentrated in vacuo. Purification using gradient from 0% to 100% of EtOAc in cHex rendered **11a** (288 mg, 28%). LCMS (ESI): Rt = 4.70 min, m/z = 520.00 [M+ H]⁺.

4.2.4. *7-[6-(5-Amino-6-methoxy-pyridin-3-yl)-quinolin-4-yl]-3,4-dihydro-1H-isoquinoline-2-carboxylic acid tert-butyl ester (15).*

Compound **10a** (250 mg, 0.875 mmol), 2-(tert-butoxycarbonyl)-1,2,3,4-tetrahydroisoquinolin-7-yl-7-boronic acid (303 mg 1.094 mmol) and PdCl₂(PPh₃)₂ (61 mg 0.087 mmol) in 1,4-dioxane (3.5 mL) and Na₂CO₃ (aq sat sol, 1.75 mL) were heated at 115 °C in pressure tube overnight. The mixture was partitioned between EtOAc and water. Layers were separated and the aqueous phase was extracted with EtOAc. Combined organic extract was dried (Na₂SO₄), filtered and concentrated. Purification by column

chromatography on silica gel with gradient solvent from 0% to 100% of EtOAc in DCM afforded **15** (yellow foam, 350 mg, 83%). LCMS (ESI): Rt = 4.60 min, m/z = 483.30 [M+ H]⁺.

4.2.5. *{5-[6-(5-Amino-6-methoxy-pyridin-3-yl)-[1,5]naphthyridin-4-yl]-pyridin-3-yl methyl}-carbamic acid tert-butyl ester (**16**).*

Compound **10b** (259 mg, 0.903 mmol), 3-(N-Boc-aminomethyl)pyridine-5-boronic acid pinacol ester (381 mg, 1.084 mmol) and PdCl₂(PPh₃)₂ (32 mg, 0.045 mmol) in 1,2-DME (3.01 mL) and Na₂CO₃ (aq sat sol, 1.51 mL) were heated at 80 °C in pressure tube for 30 min. The reaction mixture was concentrated. Purification by column chromatography on silica gel with gradient solvent from 0% to 100% of EtOAc in cHex and then gradient from 0% to 30 % of MeOH in EtOAc gave pure compound **16** (73 mg, 18%). LCMS (ESI): Rt = 3.96 min, m/z = 459.20 [M+ H]⁺.

4.2.6 *5-(5-{4-[5-(tert-Butoxycarbonylamino-methyl)-pyridin-3-yl]-quinolin-6-yl}-2-methoxy-pyridin-3-ylsulfamoyl)-2,4-difluoro-benzoic acid (**25**).*

From **11a** (350 mg, 0.673 mmol), 3-(N-Boc-aminomethyl)pyridine-5-boronic acid pinacol ester (276 mg, 0.808 mmol), Pd(PPh₃)₄ (79 mg, 0.067 mmol) in 1,4-dioxane (5.4 mL) and K₂CO₃ 1M (2.8 mL) heated at 100 °C for 1 h. Purification using gradient from 0% to 20% of MeOH in EtOAc afforded **25** (300 mg, 66%). LCMS (ESI): Rt = 4.18 min, m/z = 678.2 [M+ H]⁺. ¹H NMR (300 MHz, DMSO-*d*₆) δ 8.99 (d, *J* = 4.4 Hz, 1H), 8.70 (d, *J* = 1.9 Hz, 1H), 8.64 (d, *J* = 1.9 Hz, 1H), 8.21 (d, *J* = 8.7 Hz, 2H), 7.92 (s, 2H), 7.54 (d, *J* = 4.4 Hz, 2H), 4.30 (d, *J* = 5.6 Hz, 2H), 3.69 (s, 3H), 1.32 (s, 9H).

4.2.7. *3-(5-{8-[5-(tert-Butoxycarbonylamino-methyl)-pyridin-3-yl]-[1,5]naphthyridin-2-yl}-2-methoxy-pyridin-3-ylsulfamoyl)-benzoic acid (**36**).*

Compound **12b** (220 mg, 0.467 mmol), 3-(N-Boc-aminomethyl)pyridine-5-boronic acid pinacol ester (197 mg, 0.561 mmol), PdCl₂(PPh₃)₂ (16 mg, 0.023 mmol) and Na₂CO₃ (aq sat. sol., 0.80 mL) in 1,2-DME (1.6 mL) were heated at 80 °C for 1 h in a seal tube. The mixture was concentrated. Purification by column chromatography on silica gel with gradient solvent from 0% to 100% of EtOAc in cHex and then gradient from 0% to 30% of MeOH in EtOAc afforded the title compound **36** (206 mg, 51%). LCMS (ESI): Rt = 4.02 min, m/z = 643.2 [M+ H]⁺. ¹H NMR (300 MHz, DMSO-*d*₆) δ 9.07 (d, *J* = 4.4 Hz, 1H), 8.98 (s, 1H), 8.78 (s, 1H), 8.62 (s, 1H), 8.57 (d, *J* = 8.9 Hz, 1H), 8.42 (d, *J* = 9.1 Hz, 1H), 8.35 (s, 1H), 8.31 (s, 1H), 8.15 (s, 1H), 8.08 (d, *J* = 7.8 Hz, 1H), 7.90 (d, *J* = 4.4 Hz, 1H), 7.79 (d, *J* = 7.7 Hz, 1H), 7.55 (t, *J* = 7.8 Hz, 1H), 7.48 (s, 1H), 4.34 (d, *J* = 5.9 Hz, 2H), 3.64 (s, 3H), 1.34 (s, 9H).

4.2.8. *{2-[4-(6-Bromo-quinazolin-4-yl)-pyrazol-1-yl]-ethyl}-carbamic acid tert-butyl ester (97)*.

To a reaction vessel was added a mixture of {2-[4-(4,4,5,5-Tetramethyl-[1,3,2]dioxaborolan-2-yl)-pyrazol-1-yl]-ethyl}-carbamic acid tert-butyl ester (0.73 g, 2.16 mmol), compound **8** (0.50 g, 2.06 mmol), Pd(dppf)Cl₂ (84 mg, 0.10 mmol), and Na₂CO₃ (0.65 g, 6.17 mmol) in a solution of DME (8 mL) and H₂O (2.5 mL). The reaction vessel was sealed and heated in microwave at 140 °C for 40 min. The reaction mixture was poured into water, extracted with EtOAc, the organic layer was washed with brine, dried over Na₂SO₄, concentrated. The residue was purified by chromatography column on silica gel to give compound **97** (125 mg, 15 %).

4.2.9. *(2-[4-[6-(5-Amino-6-methoxy-pyridin-3-yl)-quinazolin-4-yl]-pyrazol-1-yl]-ethyl)-carbamic acid tert-butyl ester (103)*.

Compound **97** (3 g, 7.1 mmol), (5-amino-6-methoxypyridin-3-yl)boronic acid pinacol ester (2.2 g, 8.9 mmol), Pd(PPh₃)₄ (0.46 g, 0.41 mmol) and K₂CO₃ (3.4 g, 24.4 mmol) in a mixture of 1,4-dioxane:H₂O (150 mL:50 mL) was stirred under N₂ at reflux for 2 h. The mixture was cooled to rt and extracted with EtOAc (100 mL x 3). The organic layers were combined, washed with brine, dried over Na₂SO₄, filtered and concentrated. The residue was purified by column chromatography on silica gel with gradient from 10% to 60% of EtOAc in phenylether to give the title compound **103** as yellow solid (2 g, 60%).

4.3. Synthesis of intermediates by sulfonamide formation

4.3.1. 3-[5-(8-Chloro-[1,5]naphthyridin-2-yl)-2-methoxy-pyridin-3-ylsulfamoyl]-benzoic acid (**12b**).

Compound **10b** (1.363 g, 4.754 mmol), 3-(chlorosulfonyl)benzoic acid (1.325 g, 5.705 mmol) in pyridine (44 mL) was stirred for 25 min. The reaction was quenched with MeOH, concentrated and purified by column chromatography with gradient solvent from 0% to 100% of EtOAc in c-Hex and then gradient from 0% to 20 % of MeOH in EtOAc to afford **12b** (537 mg, 24%). LCMS (ESI): Rt = 4.28 min, m/z = 471.20 [M+ H]⁺. ¹H NMR (300 MHz, DMSO-*d*₆) δ ppm 8.89 (d, *J* = 4.6 Hz, 2H), 8.53 (m, 3H), 8.42 (s, 1H), 8.16 (d, *J* = 7.8 Hz, 1H), 8.07 – 8.01 (m, 2H), 7.69 (t, *J* = 7.8 Hz, 1H), 3.76 (s, 3H).

4.3.2. 7-{6-[5-(3-Carboxy-benzenesulfonylamino)-6-methoxy-pyridin-3-yl]-quinolin-4-yl}-3,4-dihydro-1H-isoquinoline-2-carboxylic acid tert-butyl ester (**27**).

Compound **15** (425 mg, 0.881 mmol) and 3-(chlorosulfonyl)benzoic acid (291 mg, 1.321 mmol) were dissolved in pyridine (9 mL) at -20 °C and stirred for 2 h, at rt. The reaction mixture was quenched with methanol and solvents were removed under *vacuum*. The residue was purified by column chromatography on silica gel with gradient from 0% to

15% of MeOH in DCM to afford compound **27** (420 mg, 70%). LCMS (ESI): Rt = 4.64 min, m/z = 667.2 [M+ H]⁺.

4.3.3. *(5-{8-[5-(tert-Butoxycarbonylamino-methyl)-pyridin-3-yl]-[1,5]naphthyridin-2-yl}-2-methoxy-pyridin-3-yl)sulfamoyl)-2,4-difluoro-benzoic acid (35)*.

Compound **16** (190 mg, 0.414 mmol) and methyl 5-(chlorosulfonyl)-2,4-difluorobenzoate (135 mg, 0.497 mmol) were mixed in pyridine (3 mL) at 0 °C. The reaction mixture was stirred for 30 min at 0 °C and quenched with MeOH. The solvent was evaporated *in vacuum* and the residue was purified by column chromatography with gradient of 0% to 100% of EtOAc in cHex to give 5-(5-{8-[5-(tert-Butoxycarbonylamino-methyl)-pyridin-3-yl]-[1,5]naphthyridin-2-yl}-2-methoxy-pyridin-3-yl)sulfamoyl)-2,4-difluoro-benzoic acid methyl ester (88 mg, 31%). The benzoic acid methyl ester derivative was treated with K₂CO₃ (53 mg, 0.381 mmol) in 1,4-dioxane (1.3 mL) and water (0.42 mL) stirring at 100 °C for 3 h. The solvent was concentrated *in vacuum* and the crude was purified by column chromatography on silica gel with gradient from 0% to 100% of EtOAc in cHex followed by gradient from 0% to 40% of MeOH in EtOAc to give compound **35** (50 mg). LCMS (ESI): Rt = 4.87 min, m/z = 679.2 [M+ H]⁺. ¹H NMR (300 MHz, DMSO-*d*₆) δ 9.05 (d, *J* = 4.4 Hz, 1H), 8.96 (s, 1H), 8.62 – 8.56 (m, 1H), 8.53 (s, 1H), 8.18 (m, 3H), 8.15 (s, 1H), 7.88 (d, *J* = 4.5 Hz, 1H), 7.48 (m, 1H), 7.37 (m, 1H), 4.33 (d, *J* = 6.1 Hz, 2H), 3.72 (s, 3H), 1.29 (s, 9H).

4.3.4. *3-(5-{4-[1-(2-tert-Butoxycarbonylamino-ethyl)-1H-pyrazol-4-yl]-quinazolin-6-yl}-2-methoxy-pyridin-3-yl)sulfamoyl)-benzoic acid (109)*.

Compound **103** (1 g, 2.800 mmol) in pyridine (10 mL) was added to a solution of 3-(chlorosulfonyl)benzoic acid (730 mg, 3.300 mmol) in DCM (50 mL) at 0 °C under N₂. The mixture was heated under reflux conditions for 18 h. MeOH was added, and the reaction

mixture was concentrated under reduced pressure. The residue was crystallized to give **109** (white solid, 600 mg, 43%).

4.4. Synthesis of intermediates by Boc deprotection

4.4.1. 5-{5-[4-(5-Aminomethyl-pyridin-3-yl)-quinolin-6-yl]-2-methoxy-pyridin-3-ylsulfamoyl}-2,4-difluoro-benzoic acid (**47**).

To a solution of **25** (280 mg, 0.413 mmol) in DCM (3 ml) at 0°C was added dropwise TFA (5.3 ml). The mixture was stirred for 40 min at rt and the solvent was concentrated in vacuo and coevaporated with toluene to yield desired compound **47** which was used in next reaction step without further purification. LCMS (ESI): Rt = 2.37 min, m/z = 578.1 [M+ H]⁺. ¹H NMR (300 MHz, DMSO-*d*₆) δ 10.55 (s, 1H), 9.05 (d, *J* = 4.4 Hz, 1H), 8.89 (d, *J* = 2.0 Hz, 1H), 8.85 (d, *J* = 2.0 Hz, 1H), 8.43 (d, *J* = 2.3 Hz, 1H), 8.28 – 8.24 (m, 2H), 8.18 (dd, *J* = 17.2, 9.3 Hz, 2H), 8.01 (d, *J* = 2.3 Hz, 1H), 7.98 (s, 1H), 7.72 (t, *J* = 10.3 Hz, 1H), 7.60 (d, *J* = 4.5 Hz, 1H), 7.29 – 7.21 (m, 2H), 7.20 – 7.10 (m, 2H), 4.25 (q, *J* = 5.5 Hz, 2H), 3.65 (s, 3H).

4.4.2. 3-{2-Methoxy-5-[4-(1,2,3,4-tetrahydro-isoquinolin-7-yl)-quinolin-6-yl]-pyridin-3-ylsulfamoyl}-benzoic acid (**49**).

Compound **27** (230 mg, 0.340 mmol) in DCM (5 mL) was treated with TFA (1.60 mL, 20.690 mmol), and the mixture was stirred at rt for 30 min. Then, the reaction was concentrated under vacuum, and the residue was further dried by co-evaporation with toluene. The resulting residue was dried under vacuum overnight rendering **49** as the trifluoroacetic acid salt which was used in the next reaction step without additional treatment.

LCMS (ESI): Rt = 2.85 min, m/z = 567.20 [M+ H]⁺. ¹H NMR (300 MHz, DMSO-*d*₆) δ ppm 8.93 (d, *J* = 4.3 Hz, 1H), 8.18 (d, *J* = 6.4 Hz, 1H), 8.13 (m, 2H), 8.01 (d, *J* = 8.5 Hz,

1H), 7.92 (d, $J = 7.8$ Hz, 1H), 7.77 (d, $J = 7.5$ Hz, 1H), 7.70 (s, 1H), 7.51 (s, 1H), 7.39 (t, $J = 9.8$ Hz, 5H), 4.30 (s, 2H), 3.80 (s, 3H), 3.40 (s, 2H), 3.15 (s, 2H).

4.4.3. *5-{5-[8-(5-Aminomethyl-pyridin-3-yl)-[1,5]naphthyridin-2-yl]-2-methoxy-pyridin-3-ylsulfamoyl}-2,4-difluoro-benzoic acid (59)*.

TFA (0.90 mL) was added dropwise to a solution of **35** (50 mg, 0.074 mmol) in DCM (0.58 mL) at 0°C. The reaction was stirred at rt for 40 min. Then, the reaction mixture was concentrated under vacuum and coevaporated 3 times with toluene affording **59** (yellow solid, 96 mg) as trifluoroacetic acid salt which was used in the next step without further purification. LCMS (ESI): $R_t = 3.83$ min, $m/z = 579.10$ $[M+H]^+$.

4.4.4. *3-{5-[8-(5-Aminomethyl-pyridin-3-yl)-[1,5]naphthyridin-2-yl]-2-methoxy-pyridin-3-ylsulfamoyl}-benzoic acid (60)*.

TFA (3.77 mL) was added dropwise to a solution of **36** (206 mg, 0.321 mmol) in DCM (2.50 mL) at 0 °C. The reaction mixture was stirred at rt for 20 min. Then, the reaction mixture was concentrated under vacuum and coevaporated 3 times with toluene affording **60** (yellow oil) as trifluoroacetic acid salt which was used in the next step without further purification. LCMS (ESI): $R_t = 2.94$ min, $m/z = 543.10$ $[M+H]^+$.

4.4.5. *3-(5-{4-[1-(2-Amino-ethyl)-1H-pyrazol-4-yl]-quinazolin-6-yl}-2-methoxy-pyridin-3-ylsulfamoyl)-benzoic acid (115)*.

TFA (5.60 mL) was added dropwise to a solution of **109** (300 mg, 0.465 mmol) in DCM (3.64 mL) at 0 °C. The reaction mixture was stirred at rt for 20 min. Then, the reaction mixture was concentrated under vacuum and coevaporated 3 times with toluene affording compound **115** (yellow oil) as trifluoroacetic acid salt which was used in the next step without further purification. LCMS (ESI): $R_t = 3.03$ min, $m/z = 546.10$ $[M+H]^+$.

4.5. *Synthesis of Macrocycles*

*6*⁴,*6*⁶-difluoro-*3*⁶-methoxy-5-thia-4,8-diaza-2(4,6)-quinolina-1,3(3,5)-dipyridina-6(1,3)-benzenacyclononaphan-7-one 5,5-dioxide (**MCX-71**). Compound **47** (0.413 mmol) was dissolved in DMF (17 ml) and DIPEA (0.861 ml, 4.955 mmol) was added. Then the mixture was added during 8 h (using a syringe pump) to a solution of PyBOP (241 mg, 0.454 mmol) and DMAP (56 mg, 0.454 mmol) in DMF (64 ml). After the addition, the mixture was stirred at rt for 8 h. the solvent was evaporated and the resulting residue was purified using gradient from 0% to 100% EtOAc in cHex and then gradient from 0% to 10% of MeOH in EtOAc and additional trituration with MeOH and ACN gave **71** (white crystalline solid, 61 mg, 26%). LCMS (ESI): Rt = 3.96 min, m/z = 560.10 [M+ H]⁺. ¹H NMR (300 MHz, DMSO-*d*₆) δ ppm 10.47 (s, 1H), 9.14 (t, *J* = 5.4 Hz, 1H), 9.02 (d, *J* = 4.4 Hz, 1H), 8.74 (dd, *J* = 5.3, 2.0 Hz, 2H), 8.22 (d, *J* = 8.7 Hz, 1H), 8.03 – 7.95 (m, 3H), 7.79 – 7.64 (m, 3H), 7.60 (d, *J* = 4.4 Hz, 1H), 7.55 (d, *J* = 1.8 Hz, 1H), 4.52 (d, *J* = 5.5 Hz, 2H), 3.77 (s, 3H). ¹³C NMR / DEPT135 (75 MHz, DMSO) δ 161.40, 158.27, 157.34, 150.45 (CH), 149.59 (CH), 148.43 (CH), 147.47, 143.71, 142.85 (CH), 136.95 (CH), 136.33, 134.21, 132.95, 132.84 (d, ³*J*_{CF} = 3.7 Hz, CH), 132.80 (CH), 130.50, 130.32 (CH), 129.69 (CH), 125.68, 123.68 (CH), 123.72, 123.23 (dd, ²*J*_{CF} and ⁴*J*_{CF} = 15.6, 5.1 Hz), 122.38 (CH), 119.64 (d, *J* = 3.5 Hz), 119.35, 106.83 (t, ²*J*_{CF} = 27.1 Hz, CH), 53.59 (CH₃), 40.24 (CH₂).

*1*⁶-methoxy-*3*¹,*3*²,*3*³,*3*⁴-tetrahydro-6-thia-7-aza-2(6,4),3(7,2)-diquinolina-1(3,5)-pyridina -5(1,3)-benzenacycloheptaphan-4-one 6,6-dioxide (**MCX-73**). The intermediate **49** (215 mg, 0.315 mmol) and DIPEA (5 eq, 1.59 mmol, 0.28 mL) in DMF (16 mL) was added *via* syringe pump (2 mL/h) to a solution of: HATU (2 eq, 0.636 mmol, 242 mg) and HOAt (sol 0.5M, 2 eq, 0.636 mmol, 1.27 mL) in DMF (48 mL). After complete addition of starting material, the reaction mixture was further stirred overnight. The solvent was removed under *vacuum*. The crude product was precipitated from methanol and washed

thoroughly with acetonitrile to render pure required macrocycle **73** (off-white solid, 59 mg, 34%). LCMS (ESI): Rt = 4.46 min, m/z = 549.30 [M+ H]⁺. ¹H NMR (300 MHz, DMSO-*d*₆) δ ppm 10.18 (s, 1H), 8.91 (d, J = 4.4 Hz, 1H), 8.45 (d, J = 2.1 Hz, 1H), 8.16 (q, J = 8.8 Hz, 2H), 7.96 (m, 1H), 7.91 (s, 1H), 7.76 (s, 2H), 7.75 (s, 1H), 7.66 (d, J = 2.2 Hz, 1H), 7.47 (d, J = 3.0 Hz, 3H), 7.43 (s, 1H), 4.54 (s, 2H), 4.02 (s, 3H), 3.93 (m, 2H), 3.08 (s, 2H). ¹³C NMR / DEPT135 (75 MHz, DMSO) δ 168.50, 157.79, 150.71 (CH), 148.21, 147.26, 142.61, 142.38 (CH), 138.10, 135.54, 135.09, 134.82, 133.42, 131.06 (CH), 130.92 (2 CH), 130.82 (CH), 129.40 (CH), 129.00, 128.35 (CH), 128.03 (CH), 128.01 (CH), 127.00 (CH), 126.15, 123.70 (CH), 122.59 (CH), 122.33 (CH), 121.53, 54.48 (CH₃), 49.68 (CH₂), 40.37 (CH₂), 27.70 (CH₂).

*6*⁴,*6*⁶-difluoro-*3*⁶-methoxy-5-thia-4,8-diaza-2(8,2)-naphthyridina-1,3(3,5)-dipyridina-6(1,3)-benzenacyclononaphan-7-one 5,5-dioxide (**MCX-83**). The crude **59** (96 mg, 0.074 mmol) was dissolved in DMF (3.1 mL) and DIPEA (0.12 mL, 0.693 mmol) was added. The mixture was slowly added (syringe pump; 2 mL/h) to a solution of HATU (56 mg, 0.148 mmol) and HOAt (0.5 M in DMF, 0.3 mL, 0.148 mmol) in DMF (11.7 mL). After the addition, the reaction was stirred for 8 h and evaporated. The residue was purified by column chromatography on silica gel with gradient from 30% to 100% of EtOAc in cHex and from 0% to 20% of MeOH in EtOAc. Additional trituration of the resulting solid with Acetonitrile and MeOH gave **83** as a white solid (3.6 mg, 9%). LCMS (ESI): Rt = 3.85 min, m/z = 561.2 [M+ H]⁺. ¹H NMR (300 MHz, DMSO) δ 10.44 (s, 1H), 9.14 (t, J = 6.2 Hz, 1H), 9.09 (d, J = 4.4 Hz, 1H), 8.82 (d, J = 2.2 Hz, 1H), 8.66 (d, J = 2.2 Hz, 1H), 8.60 (d, J = 8.7 Hz, 1H), 8.28 (d, J = 8.8 Hz, 1H), 8.14 – 8.01 (m, 2H), 7.90 (d, J = 4.5 Hz, 1H), 7.68 (t, J = 10.1 Hz, 1H), 7.33 (t, J = 7.2 Hz, 1H), 4.50 (d, J = 6.1 Hz, 2H), 3.64 (s, 3H).

^{13}C NMR / DEPT135 (75 MHz, DMSO) δ 161.48, 158.90, 155.57, 151.23 (CH), 149.13 (CH), 148.09 (CH), 145.09 (CH), 143.78, 142.91, 140.61, 139.22 (CH), 138.51 (CH), 135.02 (CH), 133.87, 133.23 (d, $^3J_{CF} = 3.8$ Hz, CH), 132.46, 129.90, 124.73 (CH), 123.70 (CH), 119.19 (dd, $^2J_{CF}$ and $^4J_{CF} = 15.9, 3.9$ Hz, 2C), 118.81, 118.05, 106.52 (dd, $^2J_{CF} = 28.3, 26.0$ Hz, CH), 53.52 (CH₃), 40.24 (CH₂).

3⁶-methoxy-5-thia-4,8-diaza-2(8,2)-naphthyridina-1,3(3,5)-dipyridina-6(1,3)-benzenacyclononaphan-7-one 5,5-dioxide (MCX-84). Crude **60** (410 mg, 0.321 mmol) was dissolved in DMF (14 mL) and DIPEA (0.54 mL, 3.122 mmol) was added. The reaction mixture was slowly added (syringe pump; 2 mL/h) to a solution of HOAt (0.5 M in DMF, 1.28 mL, 0.642 mmol) and HATU (249 mg, 0.642 mmol) in DMF (50 mL). After the addition, the reaction was stirred for 6 h and evaporated. The residue was purified by column chromatography on silica gel with gradient from 0% to 100% of EtOAc in cHex and from 0% to 30% of MeOH in EtOAc. Additional trituration of the resulting solid with Acetonitrile and MeOH gave **84** as a white solid (31 mg, 18%). LCMS (ESI): Rt = 3.57 min, m/z = 525.1 [M+ H]⁺. ^1H NMR (300 MHz, DMSO) δ 9.83 (s, 1H), 9.26 (t, $J = 6.1$ Hz, 1H), 9.09 (d, $J = 4.4$ Hz, 1H), 8.83 (d, $J = 2.3$ Hz, 1H), 8.67 (d, $J = 2.3$ Hz, 1H), 8.59 (d, $J = 8.7$ Hz, 1H), 8.32 – 8.17 (m, 2H), 8.08 – 7.93 (m, 4H), 7.91 (d, $J = 4.4$ Hz, 1H), 7.72 (t, $J = 7.8$ Hz, 1H), 7.59 (t, $J = 1.9$ Hz, 1H), 4.50 (d, $J = 5.9$ Hz, 2H), 3.50 (s, 3H). ^{13}C NMR / DEPT 135 (75 MHz, DMSO) δ 165.26, 158.80, 155.86, 151.14 (CH), 148.71 (CH), 147.71 (CH), 144.86 (CH), 143.83, 142.93, 140.61, 139.22 (CH), 138.51, 138.37 (CH), 134.26 (CH), 134.09, 134.01, 132.44, 131.69 (CH), 129.92, 129.39 (CH), 129.32 (CH), 125.94 (CH), 124.69 (CH), 123.83 (CH), 119.41, 53.41 (CH₃), 39.97 (CH₂).

3⁶-methoxy-1¹H-5-thia-4,8-diaza-2(4,6)-quinazolina-3(3,5)-pyridina-1(4,1)-

pyrazola-6(1,3)-benzenacyclodecaphan-7-one 5,5-dioxide (MCX-121). The crude **115** (461 mg, 0.465 mmol) was dissolved in DMF (21 mL) and DIPEA (0.61 mL, 3.494 mmol) was added. The mixture was slowly added (syringe pump; 2 mL/h) to a solution of HATU (361 mg, 0.930 mmol) and HOAt (0.5 M in DMF, 1.86 mL, 0.930 mmol) in DMF (72 mL). After the addition, the reaction was stirred for 4 h and evaporated. The residue was purified by column chromatography in silica gel with gradient from 0% to 100% of EtOAc in cHex and from 0% to 10% of MeOH in EtOAc to give **121** as a white solid (125 mg, 51%). LCMS (ESI): Rt = 4.09 min, m/z = 528.1 [M+ H]⁺. ¹H NMR (300 MHz, DMSO) δ 10.23 (s, 1H), 9.19 (s, 1H), 8.98 (t, *J* = 5.8 Hz, 1H), 8.69 (s, 1H), 8.42 (t, *J* = 1.9 Hz, 1H), 8.30 – 8.00 (m, 7H), 7.72 (t, *J* = 7.8 Hz, 1H), 7.67 (d, *J* = 2.2 Hz, 1H), 4.42 (dd, *J* = 6.7, 3.2 Hz, 2H), 3.97 (s, 3H), 3.77 (m, 2H). ¹³C NMR / DEPT (75 MHz, DMSO) δ 165.02, 160.19, 155.11, 154.55 (CH), 149.68, 140.59, 140.38 (CH), 140.24 (CH), 136.88, 135.09, 133.76 (CH), 133.23 (CH), 132.05 (CH), 130.01 (CH), 129.26 (CH), 129.13, 129.00 (CH), 126.43 (CH), 125.16 (CH), 123.11 (CH), 121.83, 121.50, 119.05, 53.96 (CH₃), 51.47 (CH₂), 39.96 (CH₂).

4.6. Biological Evaluation

4.6.1. Protein PI3 Kinase Assay

The PI3K- α kinase activity was measured by using the commercial ADP HunterTM Plus assay available from DiscoverX (#33-016), which is a homogeneous assay to measure the accumulation of ADP, a universal product of kinase activity. The enzymes, PI3K (p110 α) was purchased from Cama Biosciences (#07CBS-0402A). The assay was done following the manufacturer recommendations. Fluorescence counts were read in a Victor instrument (Perkin Elmer) with the recommended settings (544 and 580 nm as excitation and emission wavelengths, respectively). Values were normalized against the control activity included

(100 % PI3 kinase activity, without compound). These values were plotted against the inhibitor concentration and were fit to a sigmoid dose-response curve by using the Graphpad software.

The kinase activity of PI3K isoforms was measured by using the commercial PI3-kinase (h) HTRF™ assay available from Millipore, following the manufacturer recommendations. PI3K α (p110 α /p85 α) and PI3K δ (p110 δ /p85 α) were used at 100 pM; PI3K β (p110 β /p85 α) and PI3K γ isoforms (p110 γ) at 500 pM and 4 nM respectively. ATP concentration was 50 times $K_{M\text{ATP}}$: 200 μM for PI3K α and PI3K δ , 250 μM for PI3K β and 100 μM for PI3K γ . PIP2 was held at 10 μM . Values were normalized against the control activity included for each enzyme (i.e., 100% PI3K activity, without compound). These values were plotted against the inhibitor concentration and were fitted to a sigmoidal dose-response (variable slope) curve by using GraphPad Software. The obtained IC_{50} were converted to $K_{i\text{app}}$ according to Cheng-Prusoff equation for competitive inhibitors (Cheng, Y.; Prusoff, W.H. *Biochem. Pharmacol.* **1973**, 22, 3099).

The kinase activity of PI3K mutants was measured by using the commercial ADP-Glo™ Lipid Kinase assay available from Promega, following the manufacturer recommendations. PI3K (p110 α [H1047R]/p85 α) mutant was used at 1.7 nM, PI3K (p110 α [E545K]/p85 α) and PI3K (p110 α [E542K]/p85 α) mutants were used at 3 nM. PIP2:3PS lipid kinase substrate was held at 3.25 μM . Values were normalized against the control activity included for each enzyme (i.e., 100% PI3K activity, without compound). These values were plotted against the inhibitor concentration and were fitted to a sigmoidal dose-response (variable slope) curve by using GraphPad Software. The obtained $\text{IC}_{50\text{s}}$ were converted to $K_{i\text{app}}$

according to Cheng-Prusoff equation for competitive inhibitors (Cheng, Y.; Prusoff, W.H. *Biochem. Pharmacol.* **1973**, 22, 3099).

4.6.2. Protein mTOR Kinase Assay

mTOR (FRAP1), LanthaScreen™ Tb-anti-p4EBP1 (phosphor-threonine 46) and GFP-4EBP1 were purchased from Invitrogen. Reaction conditions used were those recommended by the manufacturer. Values given are averages of two independent experiments performed in duplicate.

4.6.3. Cell Based Assays. AKT S⁴⁷³ Phosphorylation inhibition assay (p-AKT)

Cellular activity was measured as endogenous levels of phospho-AKT1 (Ser473) protein after serum stimulation in U2OS (osteosarcoma) cells growing in 0.1% of FBS. Assay was run under C-Elisa format (Reagent: Supersignal Elisa Femto, purchased from Pierce). Values were plotted against the inhibitor concentration and fitted to a sigmoid dose-response curve using GraphPad Software.

4.6.4. PI3K/mTOR biomarkers modulation studies by Western Blot

MCF7 cells incubated for 3 h with the compounds were washed twice with PBS prior to lysis in 50 mM Tris pH 7.5, 150 mM NaCl, 1% IGEPAL CO-630, Phospho Stop (Roche) and Complete Mini EDTA (Roche). Proteins were resolved on 10% SDS-PAGE, and transferred to nitrocellulose membranes (Biorad). The membranes were incubated with antibodies against phospho-AKT (Ser473), phospho-AKT (Thr308), AKT, phospho-P70 S6Kinase (Thr389), phospho-S6 ribosomal protein (Ser235/236) and S6 Ribosomal Protein from Cell Signaling, overnight at 4 °C. After washing, blots were then incubated with secondary antibody: Alexa Fluor 680 goat anti-rabbit IgG (Invitrogen) or anti-mouse IgG DyLight 800 conjugated (Thermo Scientific), and visualized using an Odyssey infrared imaging system (Li-Cor Biosciences). For EC₅₀ calculations, western blots were quantified

with Image Studio Lite. Relative intensity was calculated considering 100% of signal corresponding to cells treated with DMSO. Values were plotted against inhibitor concentration and fitted to a sigmoid dose-response curve using GraphPad Software.

4.6.5. Antiproliferative Assay.

Cells were harvested just before reaching confluency, counted with a haemocytometer and diluted with media. Cells were then seeded in 96-well microtiter plates at a density of 4,000 cells/well. Cells were incubated for 24 h before adding the compounds. Compounds were weighed out and diluted with DMSO to a final concentration of 10 mM. From here a “mother plate” with serial dilutions was prepared at 200X the final concentration in the culture. The final concentration of DMSO in the tissue culture media should not exceed 0.5%. The appropriate volume of the compound solution (2 μ l) was added automatically (Beckman FX 96 tip) to 0.2 ml media to make it up to the final concentration for each drug. Each concentration was assayed in duplicate. Cells were exposed to the compounds for 72 h and then processed for CellTiter-Glo® Luminescent Cell Viability Assay (Promega) read out according to manufacturer’s Instruction and read on EndVision (Perkin Elmer). GI₅₀ values were calculated using ActivityBase from IDBS.

4.7. ADME-T Evaluation

4.7.1 In Vitro Microsomal Stability Assay

Human, mouse and rat microsomal stability was determined using a single time point high throughput method. The final assay conditions were: 0.5 μ M of the compounds, 0.5 mg/ml microsomal protein and NADPH-regenerating system incubated during 30 min at 37 °C. Briefly, three separate 96-well plates containing the compounds, the microsomes and the NADPH regenerating enzymatic system (REG) were prepared. In the REG plate half of

the plates contained the regenerating enzymatic system (positive wells) and half of the wells 0.1 M potassium phosphate buffer (negative wells). Parallel wells of each compound with the microsomes from all three species were prepared. The plates with the compounds, microsomes and REG were mixed with Biomek FX automated liquid-handling instrument (Beckman Coulter), adding first microsomes, second the compound and last the REG system- After 30 min incubation at 37 °C with 450 rpm shaking (Heidolph Inkubator 1000, Heidolph Titramax 1000), the reaction was stopped by adding acetonitrile containing 0.1% formic acid. The plate was centrifuged for 1 h in 4 °C at 4000 rpm with Eppendorf centrifuge 5810R. After incubation, 200 µl of supernatant was pipetted into two 96-well plates, and were analyzed with LC-MS/MS (Agilent 1100 liquid chromatographer coupled to QTRAP5500 (AB SCIEX) triple quadrupole). The data was analyzed with Analyst 1.6.2 Software.

4.7.2 *h-ERG binding Assay*

Predictor h-ERG Assay test kits were obtained from Invitrogen (Carlsbad, CA). The binding assay was carried out according to the kit instructions. Briefly, reagents were thawed and Predictor h-ERG membrane preparations were sonicated. Working 4X tracer was prepared by diluting the 250 nM stock provided in the test kit to 4 nM with h-ERG FP assay buffer also provided. Dilutions of test compounds were prepared as a 100x stocks from their final intended concentrations. Assays were performed in 384-well microplates. Aliquots (5 µL) of each concentration of test compound were pipetted into the appropriate wells of the microplate. As required, 10 µL of (2x) membrane preparation was then dispensed. Working Tracer solution (5 µL) was then added, and the plate was allowed to incubate at room temperature for at least one hour prior to measuring fluorescence

polarization. Fluorescence polarization measurements were made using an Envision Microplate Reader from PerkinElmer (Massachusetts). Measurements were made from the top using the tungsten light source. Both parallel and perpendicular fluorescence were measured using the same 530/25-excitation, and a 590/35-emission filters along with a 550 nm cut off dichroic mirror. The PMT sensitivity setting was set automatically such that the positive control well had a raw fluorescence value for the parallel signal of 50,000 relative fluorescent units (RFU). Polarization values were calculated automatically using Activity base from IDBS.

4.7.3. CYP450 Assay

The inhibition potency of compounds on CYP1A2, CYP3A4, CYP2C9, CYP2C19 and CYP2D6 activity was measured by the P450-Glo™ assay kit (Promega) with Luciferin-ME, Luciferin-PPXE, Luciferin-H, LuciferinH-EG and Luciferin-ME-EG respectively as substrates following the manufacture's protocol. Each CYP enzyme can catalyze the respective luminogenic substrate into luciferin product capable of the produce light. The reaction was initiated by the incubation of CYP enzyme, luciferin substrate and 10µM of compounds in serial dilutions 1/3 in 0.5% DMSO in 384-well Optiplate (PerkinElmer). After 5 min preincubation, NADPH regeneration reagent was added and reaction was incubated at 37 °C. After 60 min, reconstituted luciferin detection reagent was added to the reaction mixture. After 30 min, the luminescence signal was measured by Envision (Perkin Elmer). The net luminescence signals were calculated by the subtraction of background luminescence values.

4.8. Docking studies

In order to model the plausible binding mode of compound MCX **83** inside both PIK3CG and mTOR, docking studies were performed by the Induced Fit Docking (IFD) method from Schrödinger (Schrödinger Release 2020-2) [1]. IFD includes both receptor and ligand flexibility providing an accurate complex for known active compounds that cannot be docked with other traditional methods (rigid receptor). Previously, conformational sampling of the macrocycle was explored by using the Macrocycle sampling from Prime [2]. The extended sampling protocol were applied using the extra precision (XP) descriptor from GLIDE, using as a center of the grid box the corresponding crystalized ligand in PIK3CG (PDB ID 3L08) and mTOR (PDB ID 4JSX). The selection of the final pose was based on both scoring function and visual inspection comparing with the original crystal structures and the most stable conformation from Prime.

In case of GSK2126458 (Ompalisib), the binding mode inside of mTOR was explored by traditional docking using the XP mode of the GLIDE [3].

[1] Sherman, W.; Day, T.; Jacobson, M. P.; Friesner, R. A.; Farid, R., Novel Procedure for Modeling Ligand/Receptor Induced Fit Effects. *J. Med. Chem.*, 2006, 49, 534-553.

[2] Sindhikara, D.; Spronk, S. A.; Day, T.; Borrelli, K.; Cheney, D. L.; Posy, S. L. Improving Accuracy, Diversity, and Speed with Prime Macrocycle Conformational Sampling., *Journal of Chemical Information and Modeling* 2017 57 (8), 1881-1894. doi: 10.1021/acs.jcim.7b00052.

[3] Friesner, R. A.; Murphy, R. B.; Repasky, M. P.; Frye, L. L.; Greenwood, J. R.; Halgren, T. A.; Sanschagrin, P. C.; Mainz, D. T., Extra Precision Glide: Docking and Scoring Incorporating a Model of Hydrophobic Enclosure for Protein-Ligand Complexes. *J. Med. Chem.*, 2006, 49, 6177–6196.

Acknowledgments

We thank Isabel Reymundo and Genoveva Mateos for compound handling and sample preparation. Elena Hernández-Encinas who reanalyzed PK data. Bruno Di Geronimo who performed docking studies of GSK-2126458 in mTOR-Torin 2 complex. The Ministry of Science and Innovation (MICINN) of Spain supported this research through the project ADE08/90038.

Appendix A. Supplementary data

Additional synthetic experimental procedures; ¹HNMR and ¹³CNMR of final macrocyclic compounds; GSK-2126458 PK data (Table S1); and selectivity profile (Table S2, Table S3); and Figure S1 are detailed in the supporting information.

Notes

The authors declare no competing financial interest.

References

1. Yang, J.; Nie, J.; Ma, X.; Wei, Y.; Peng, Y.; Wei, X., Targeting PI3K in cancer: mechanisms and advances in clinical trials. *Mol Cancer* 2019, 18 (1), 26. doi: 10.1186/s12943-019-0954-x.
2. Yuan, J.; Mehta, P. P.; Yin, M. J.; Sun, S.; Zou, A.; Chen, J.; Rafidi, K.; Feng, Z.; Nickel, J.; Engebretsen, J.; Hallin, J.; Blasina, A.; Zhang, E.; Nguyen, L.; Sun, M.; Vogt, P. K.; McHarg, A.; Cheng, H.; Christensen, J. G.; Kan, J. L.; Bagrodia, S., PF-04691502, a potent and selective oral inhibitor of PI3K and mTOR kinases with antitumor activity. *Mol Cancer Ther* 2011, 10 (11), 2189-99. doi: 10.1158/1535-7163.MCT-11-0185.
3. Liu, P.; Cheng, H.; Roberts, T. M.; Zhao, J. J., Targeting the phosphoinositide 3-kinase pathway in cancer. *Nat Rev Drug Discov* 2009, 8 (8), 627-44. doi: 10.1038/nrd2926.
4. Sarbassov, D. D.; Ali, S. M.; Sabatini, D. M., Growing roles for the mTOR pathway. *Curr Opin Cell Biol* 2005, 17 (6), 596-603. doi: 10.1016/j.ceb.2005.09.009.

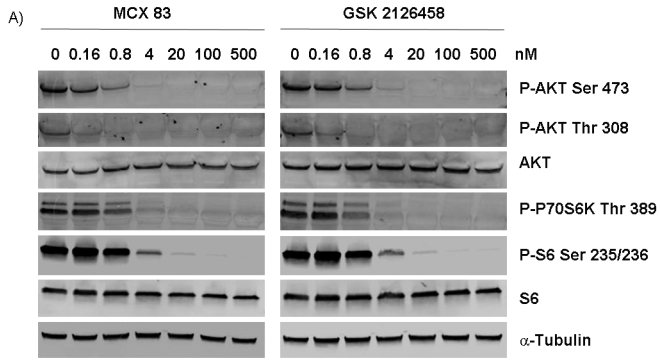
5. Dienstmann, R.; Rodon, J.; Serra, V.; Tabernero, J., Picking the point of inhibition: a comparative review of PI3K/AKT/mTOR pathway inhibitors. *Mol Cancer Ther* 2014, 13 (5), 1021-31. doi: 10.1158/1535-7163.MCT-13-0639.
6. Blachly, J. S.; Baiocchi, R. A., Targeting PI3-kinase (PI3K), AKT and mTOR axis in lymphoma. *Br J Haematol* 2014, 167 (1), 19-32. doi: 10.1111/bjh.13065.
7. Serra, V.; Markman, B.; Scaltriti, M.; Eichhorn, P. J.; Valero, V.; Guzman, M.; Botero, M. L.; Llonch, E.; Atzori, F.; Di Cosimo, S.; Maira, M.; Garcia-Echeverria, C.; Parra, J. L.; Arribas, J.; Baselga, J., NVP-BEZ235, a dual PI3K/mTOR inhibitor, prevents PI3K signaling and inhibits the growth of cancer cells with activating PI3K mutations. *Cancer Res* 2008, 68 (19), 8022-30. doi: 10.1158/0008-5472.
8. Cummings, M. D.; Sekharan, S., Structure-Based Macrocycle Design in Small-Molecule Drug Discovery and Simple Metrics To Identify Opportunities for Macrocyclization of Small-Molecule Ligands. *J Med Chem* 2019, 62 (15), 6843-6853. doi: 10.1021/acs.jmedchem.8b01985.
9. Driggers, E. M.; Hale, S. P.; Lee, J.; Terrett, N. K., The exploration of macrocycles for drug discovery-an underexploited structural class. *Nat Rev Drug Discov* 2008, 7 (7), 608-24. doi: 10.1038/nrd2590.
10. Giordanetto, F.; Kihlberg, J., Macrocyclic drugs and clinical candidates: what can medicinal chemists learn from their properties? *J Med Chem* 2014, 57 (2), 278-95. doi: 10.1021/jm400887j.
11. Marsault, E.; Peterson, M. L., Macrocycles are great cycles: applications, opportunities, and challenges of synthetic macrocycles in drug discovery. *J Med Chem* 2011, 54 (7), 1961-2004. doi: 10.1021/jm1012374.
12. Basit, S.; Ashraf, Z.; Lee, K.; Latif, M., First macrocyclic 3(rd)-generation ALK inhibitor for treatment of ALK/ROS1 cancer: Clinical and designing strategy update of lorlatinib. *Eur J Med Chem* 2017, 134, 348-356. doi: 10.1016/j.ejmech.2017.04.032.
13. Knight, S. D.; Adams, N. D.; Burgess, J. L.; Chaudhari, A. M.; Darcy, M. G.; Donatelli, C. A.; Luengo, J. I.; Newlander, K. A.; Parrish, C. A.; Ridgers, L. H.; Sarpong, M. A.; Schmidt, S. J.; Van Aller, G. S.; Carson, J. D.; Diamond, M. A.; Elkins, P. A.; Gardiner, C. M.; Garver, E.; Gilbert, S. A.; Gontarek, R. R.; Jackson, J. R.; Kershner, K. L.; Luo, L.; Raha, K.; Sherk, C. S.; Sung, C. M.; Sutton, D.; Tummino, P. J.; Wegrzyn, R. J.; Auger, K. R.; Dhanak, D., Discovery of GSK-2126458, a Highly Potent Inhibitor of PI3K and the Mammalian Target of Rapamycin. *ACS Med Chem Lett* 2010, 1 (1), 39-43. doi: 10.1021/ml900028r
14. Yang, H.; Rudge, D. G.; Koos, J. D.; Vaidialingam, B.; Yang, H. J.; Pavletich, N. P., mTOR kinase structure, mechanism and regulation. *Nature* 2013, 497 (7448), 217-23. doi: 10.1038/nature12122.
15. Martinez Gonzalez, S.; Hernandez, A. I.; Varela, C.; Lorenzo, M.; Ramos-Lima, F.; Cendon, E.; Cebrian, D.; Aguirre, E.; Gomez-Casero, E.; Albarran, M. I.; Alfonso, P.; Garcia-Serelde, B.; Mateos, G.; Oyarzabal, J.; Rabal, O.; Mulero, F.; Gonzalez-Granda, T.; Link, W.; Fominaya, J.; Barbacid, M.; Bischoff, J. R.; Pizcueta, P.; Blanco-Aparicio, C.; Pastor, J., Rapid identification of ETP-46992, orally bioavailable PI3K inhibitor, selective versus mTOR. *Bioorg Med Chem Lett* 2012, 22 (16), 5208-14. doi: 10.1016/j.bmcl.2012.06.093.
16. The generation and sampling of ligand conformations needed for docking studies is well standardized for small molecules but it is not trivial for MCXs. The conformational analysis of a given MCX could be complex since it depends on the

number of degrees of freedom, existence of intramolecular interactions, steric repulsions and ring strain effects. These aspects are so connected in MCXs that small modification in one dihedral angle can affect drastically the whole conformation. Another issue is the implementation of algorithms able to manage barriers separating local energy minimal (reference 17). Novel methods for conformational sampling of MCXs have emerged recently (Sindhikara, D.; Spronk, S.A.; Day, T.; Borrelli, K.; Cheney, D.L.; Posy, S.L. Improving Accuracy, Diversity, and Speed with Prime Macrocyclic Conformational Sampling. *J. Chem. Inf. Model.*, 2017, 57(8), 1881-1894 and www.schrodinger.com/products/macrocycles). We plan to apply them together with in depth computational studies to further understand the SAR of our PI3K/mTOR inhibitors.

17. Solomon D. Appavoo, S. D.; Huh, S.; Diaz, D.B.; Yudin, A.K. Conformational Control of Macrocycles by Remote Structural Modification. *Chem. Rev.* 2019, 119, 9724–9752. doi: 10.1021/acs.chemrev.8b00742.
18. Nishimura, N.; Siegmund, A.; Liu, L.; Yang, K.; Bryan, M. C.; Andrews, K. L.; Bo, Y.; Booker, S. K.; Caenepeel, S.; Freeman, D.; Liao, H.; McCarter, J.; Mullady, E. L.; San Miguel, T.; Subramanian, R.; Tamayo, N.; Wang, L.; Whittington, D. A.; Zalameda, L.; Zhang, N.; Hughes, P. E.; Norman, M. H., Phosphoinositide 3-kinase (PI3K)/mammalian target of rapamycin (mTOR) dual inhibitors: discovery and structure-activity relationships of a series of quinoline and quinoxaline derivatives. *J Med Chem* 2011, 54 (13), 4735-51. doi: 10.1021/jm200386s
19. Han, F.; Lin, S.; Liu, P.; Liu, X.; Tao, J.; Deng, X.; Yi, C.; Xu, H., Discovery of a Novel Series of Thienopyrimidine as Highly Potent and Selective PI3K Inhibitors. *ACS Med Chem Lett* 2015, 6 (4), 434-8. doi: 10.1021/ml5005014.
20. Beno, B. R.; Yeung, K. S.; Bartberger, M. D.; Pennington, L. D.; Meanwell, N. A., A Survey of the Role of Noncovalent Sulfur Interactions in Drug Design. *J Med Chem* 2015, 58 (11), 4383-438. doi: 10.1021/jm501853m.
21. Karoly Tihanyi, M. L. B., Eva Hellinger and Monika Vastag, CYP Inhibition-Mediated Drug-Drug Interactions. *Current Enzyme Inhibition*.2010, 6 (130). doi.org/10.2174/157340810793384106
22. Duan, J.; Tao, J.; Zhai, M.; Li, C.; Zhou, N.; Lv, J.; Wang, L.; Lin, L.; Bai, R., Anticancer drugs-related QTc prolongation, torsade de pointes and sudden death: current evidence and future research perspectives. *Oncotarget* 2018, 9 (39), 25738-25749. doi: 10.18632/oncotarget.25008
23. Beaufils, F.; Cmiljanovic, N.; Cmiljanovic, V.; Bohnacker, T.; Melone, A.; Marone, R.; Jackson, E.; Zhang, X.; Sele, A.; Borsari, C.; Mestan, J.; Hebeisen, P.; Hillmann, P.; Giese, B.; Zvelebil, M.; Fabbro, D.; Williams, R. L.; Rageot, D.; Wymann, M. P., 5-(4,6-Dimorpholino-1,3,5-triazin-2-yl)-4-(trifluoromethyl)pyridin-2-amine (PQR309), a Potent, Brain-Penetrant, Orally Bioavailable, Pan-Class I PI3K/mTOR Inhibitor as Clinical Candidate in Oncology. *J Med Chem* 2017, 60 (17), 7524-7538. doi: 10.1021/acs.jmedchem.7b00930.
24. www.discoverx.com. The selectivity score used as a quantitative measure of compound selectivity is calculated by dividing the number of kinases which compounds bind with %Ctrl < 35 by the total number of kinases tested, excluding mutant variants. The %Ctrl signal (% vs. untreated) is used as a potency threshold in this calculation

25. Yanamandra, M.; Mitra, S.; Giri, A., Development and application of PI3K assays for novel drug discovery. *Expert Opin Drug Discov* 2015, 10 (2), 171-86. doi: 10.1517/17460441.2015.997205.
26. Cheng, Y.; Prusoff, W. H., Relationship between the inhibition constant (K_i) and the concentration of inhibitor which causes 50 per cent inhibition (IC_{50}) of an enzymatic reaction. *Biochem Pharmacol* 1973, 22 (23), 3099-108. doi: 10.1517/17460441.2015.997205.

Journal Pre-proof



B)

	EC ₅₀ (nM)	
	MCX 83	GSK-2126458
P-AKT S473	0.46	0.65
P-AKT T308	0.14	0.21
P-P70 S6 T389	0.92	0.68
P-S6 S235/236	0.84	0.87

Journal Pre-proof

Highlights

- Design and synthesis of a new series of MCXs as dual PI3K/mTOR inhibitors.
- Macrocyclization strategy used to tune dual PI3K/mTOR inhibition.
- MCXs with potent biochemical, cellular activity and kinase selectivity.
- MCXs with good drug-like properties.
- MCX **83**, highly potent, selective and orally bioavailable PI3K/mTOR inhibitor.

Declaration of interests

The authors declare that they have no known competing financial interests or personal relationships that could have appeared to influence the work reported in this paper.

The authors declare the following financial interests/personal relationships which may be considered as potential competing interests:

Journal Pre-proof